https://doi.org/10.5194/wes-2026-84
Preprint. Discussion started: 20 May 2026
© Author(s) 2026. CC BY 4.0 License.



eawe european academy of wind energy
Open Access WIND ENERGY SCIENCE DISCUSSIONS

Multi-scale simulations of wind farm impacts on nighttime near-surface temperature in complex terrain

Paul Boumendil[1,2], Pierre-Antoine Joulin[1], Quentin Rodier[2], and Valéry Masson[2]

[1]IFP Energies Nouvelles, 1–4 Avenue du Bois Préau, 92852 Rueil-Malmaison, France
[2]Météo France, CNRM, 42 Avenue Gaspard Coriolis, 31057 Toulouse, France

Correspondence: Pierre-Antoine Joulin (pierre-antoine.joulin@ifpen.fr)

Abstract. Various studies have shown that wind turbine wakes can induce meteorological variations, investigating these effects near the ground is particularly important for assessing their potential impact on vegetation and human activities. In this study, the multi-scale Meso-NH/SURFEX/EOL modelling framework, which includes coupled atmosphere-soil-vegetation and actuator models, is used to investigate turbine-atmosphere interactions at the *Ensemble Éolien Catalan* wind farm during a stable nocturnal radiative cooling event associated with frost risk in nearby vineyards. The simulations are performed using nested domains to dynamically downscale the atmospheric conditions from the operational weather forecast AROME-1.3km to a horizontal resolution of 5 m, allowing explicit representation of turbine wakes through rotative actuator disk representation. Turbine-induced meteorological variations are quantified by comparing simulations performed with and without actuator model. The results reveal that near-surface meteorological responses arise from the combined influence of individual turbine wakes and the large-scale impact of the wind farm, which modifies the flow dynamic and temperature field. In the immediate vicinity of the farm, a mean near-surface warming of approximately 0.4 °C is found, with localized temperature increases reaching up to 1.6 °C in the near wake of individual turbines. The strongest perturbations occur for turbines located within valleys, where strong temperature inversions enhance turbine-induced thermal variation. In addition, the wind farm shifts the position of a convergence zone associated with a katabatic flow by about 100–400 m, producing warming anomalies of up to 2 °C along the displaced meteorological front.

1 Introduction

The expansion in both the size and number of wind turbines within wind farms raises increasing concerns about their potential meteorological impacts. Field measurements campaigns (Archer et al., 2019; Rajewski et al., 2013; Smith et al., 2013), numerical simulations (Baidya Roy et al., 2004; Xie and Archer, 2017; Wu et al., 2023; Adkins and Sescu, 2018; Joulin et al., 2020) and satellite measurements (Zhou et al., 2012) have revealed measurable modifications in temperature and humidity parameters downstream of wind farms. The sign and magnitude of these meteorological variations appear to be primarily governed by the thermal structure of the atmosphere (Archer et al., 2019; Wu and Archer, 2021), and thus by its stability. Under stable conditions, near-ground air temperature increases up to +2 °C have been reported between the upstream and downstream regions of wind farms (Henschen et al., 2011). In contrast, under unstable stratification, studies report either no significant change or

https://doi.org/10.5194/wes-2026-84
Preprint. Discussion started: 20 May 2026
© Author(s) 2026. CC BY 4.0 License.



eawe european academy of wind energy
Open Access WIND ENERGY SCIENCE DISCUSSIONS

a weak cooling effect up to -0.7 °C (Rajewski et al., 2013). Those enhanced nighttime temperatures and increased vertical mixing may reduce dew duration and modify moisture availability, potentially impacting crop respiration, photosynthesis, and soil decomposition rates (Armstrong et al., 2014; Adkins and Sescu, 2017). Consistently, the economic study of (Kaffine, 2019) reported a positive correlation between wind farm development and crop productivity, suggesting that wind-farm-induced micro climatic changes may contribute to improved growing conditions. Wind farm have also been linked to mixed impacts on vegetation cover, plant growth and diversity, depending on regional climate and land-use conditions. While some other studies report reduced vegetation grow (Tang et al., 2017) or species diversity primarily due to land disturbance during construction and incomplete ecological recovery (Urziceanu et al., 2021), others observe neutral or even positive effects, such as enhanced vegetation growth under arid conditions linked to reduced evapotranspiration (Qin et al., 2022). These atmospheric modifications are not only relevant for understanding the environmental footprint of wind farms but also have implications for their operational performance. Changes in temperature and therefore stability can affect downstream turbine loads, wake recovery, and power production (Rajewski et al., 2013; Porté-Agel et al., 2020). Consequently, a comprehensive understanding of wind turbine-atmosphere-surface interactions across all scales is essential to assess both the energy and environmental aspects of wind turbines.

In order to investigate this phenomena and its mechanisms, numerical studies have been conducted using roughness-length (Keith et al., 2004) and farm parameterizations (Baidya Roy et al., 2004; Baidya Roy and Traiteur, 2010; Baidya Roy, 2011; Quint et al., 2025) to model the effects of wind turbines. By the large-scale nature of the first studies on this subject, such effects were primarily attributed to the turbulent kinetic energy (TKE) added by the wind turbines wake, which enhances vertical mixing. To gain further insight into the micro scale mechanisms, high-resolution Large-Eddy Simulations (LES) coupled with actuator models have been used to allow a good fidelity representation of individuals wake structure. Those new studies showed that the vertical movement induce by the counter-rotation of the wake in response to the blade rotation (Wu and Porté-Agel, 2011; Mirocha et al., 2014) can disrupts the natural atmospheric stratification. These local anomalies are then advected by the wind, resulting in temperature and humidity variations that can extend well below the rotor area (Adkins and Sescu, 2017; Xie and Archer, 2017; Joulin et al., 2020; Boumendil et al., 2024, 2025). These studies highlight the need for turbine parameterizations that explicitly account for rotational effects, as the blade and wake rotation plays a key role in the vertical movements and in the resulting meteorological modifications (Boumendil et al., 2024). At the same time, the VERTEX field campaign (Archer et al., 2019) and recent Large Eddy Simulation (LES) studies (Wu et al., 2023) have shown that near the surface, temperature variations can occur even in the absence of increased turbulent kinetic energy (TKE) and may even coincide with a reduction of TKE. This challenges the hypothesis that enhanced vertical mixing is the only mechanism driving near-ground temperature changes in turbine wakes. Instead, (Archer et al., 2019; Wu et al., 2023) suggest that, in the presence of turbine wakes, the vertical convergence of turbulent heat flux below hub height plays a dominant role in driving near-surface temperature changes. Overall, these results highlight the importance of the spatial scale at which the phenomenon is investigated in determining the underlying physical mechanisms. Coherent vertical movements within individual turbine wakes, which are resolved in LES, may appear only as added TKE in large-scale simulations using farm parameterizations.

https://doi.org/10.5194/wes-2026-84
Preprint. Discussion started: 20 May 2026
© Author(s) 2026. CC BY 4.0 License.



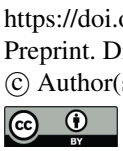
eawe european academy of wind energy
Open Access WIND ENERGY SCIENCE DISCUSSIONS

While the coupling between LES simulation and actuators methods provide valuable information on wake dynamics and turbulence, the LES are most often performed under idealized and stationary conditions, with prescribed initial uniform atmospheric states. Such simplifications neglect the dynamic nature of the real atmosphere, which continuously evolves across spatial and temporal scales in terms of stability, turbulence, fluxes, wind speed, and direction. They also neglect the heterogeneity of the the surface in terms of orography, change in rugosity and land cover. Yet, these factors through the atmospheric and surface properties critically determine the wake behavior and its potential impact on the near surface air (Porté-Agel et al., 2020). To account for these different processes in our study, we employ a multi-scale online coupling approach, referred to as Meso-NH/SURFEX/EOL. This framework combines the LES atmospheric model Meso-NH (Lac et al., 2018) with the SURFEX land surface scheme to represent soil, vegetation, and surface fluxes (Masson et al., 2013). The wind turbines are represented using actuator methods implemented in the EOL module of Meso-NH (Joulin et al., 2020). Since wake rotational effects have been shown to be an important contributor to near-surface temperature changes (Boumendil et al., 2024), the actuator disk model with rotation (ADR) is used. Because the atmospheric flow is dynamic and unsteady, ADR operation is driven by a controller that dynamically adjusts the rotational speed, blade pitch angle, and nacelle yaw direction.

This type of couplings have been used in the past especially with WRF, particularly to study wind turbine (Mi et al., 2025; Kale et al., 2023; Wise et al., 2022) and wind farm (Wang et al., 2020; Rasheed et al., 2017) interactions with complex terrain or specific atmospheric phenomena (Bakhoday-Paskyabi et al., 2022). Using grid-nested domains, it simulate scales ranging from the mesoscale, capturing diurnal cycles, to the microscale, resolving the flow behavior around wind turbines while accounting for realistic features such as orography, surface cover, clouds, and radiation. In our previous work (Boumendil et al., 2025), this multi-scale coupling framework was developed and validate with the VERTEX measurement campaign (Archer et al., 2019) with a single-turbine configuration, demonstrating its ability to reproduce realistic atmosphere for different stability conditions and to capture the interaction between turbine wakes and transitioning boundary-layer. That study established the methodology and validated the Meso-NH/SURFEX/EOL multi-scale setup. In the present paper, we extend this approach to a real wind farm located near Perpignan (France) call *Ensemble Éolien Catalan* place within the vineyards of Languedoc. The objective is to investigate the combined effects of multiple turbines within the farm on local meteorological conditions, with particular attention to the near-ground atmospheric response. The study aims to determine how the spatial organization of the turbines and the evolving mesoscale environment jointly influence meteorological change induce by the wind turbines.

Previous studies have shown that the most pronounced wind-turbine-induced near ground meteorological variations occur under stable atmospheric conditions, when the near-ground temperature lapse rate is high. In such situations, turbines wake vertical movements can significantly alter the naturally stratified structure of the nocturnal boundary layer. To investigate a case characterized by a strong nocturnal temperature inversion, we select the night 7–8 April 2021, during which nocturnal frost events were reported across Europe, affecting 80 % of the fruit orchards and vineyards in France (Lamichhane, 2021). A mean of protection used by winemakers consist of small fans tower to mix the near-surface air. The idea is to blow the ground cold layer of air and enhance sensible heat transfer from the air to the plants (Snyder and de Melo-Abreu, 2005). In this context, we aim to evaluate how the *Ensemble Éolien Catalan* wind farm interacts with the stable atmosphere shaped by

https://doi.org/10.5194/wes-2026-84
Preprint. Discussion started: 20 May 2026
© Author(s) 2026. CC BY 4.0 License.



eawe european academy of wind energy
Open Access WIND ENERGY SCIENCE DISCUSSIONS

the surrounding complex terrain, and how it may locally increase near-surface temperatures and potentially contribute to the mitigation of nocturnal frost over the surrounding vineyards.

2 Case study

This section presents the characteristics of the selected wind farm and its surrounding environment. The meteorological conditions of the study period are then described.

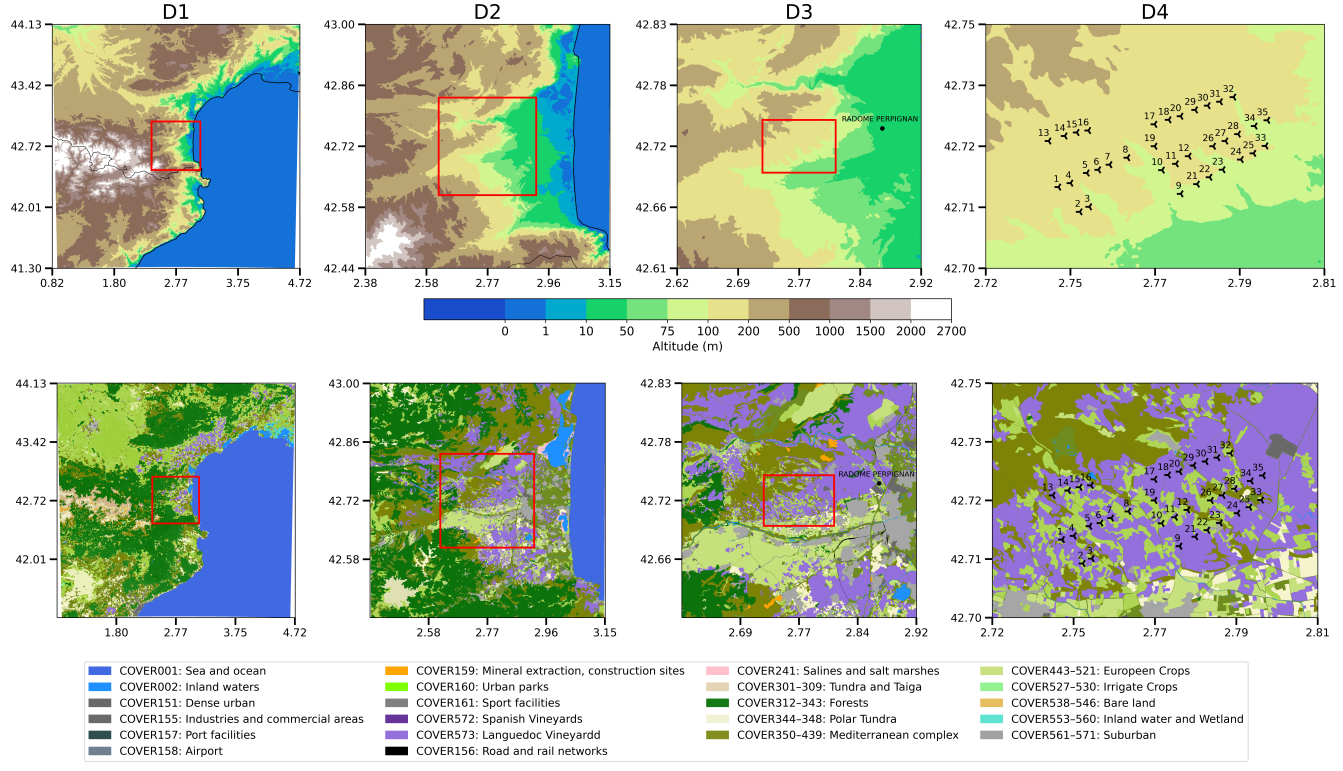


Figure 1. Ground orography (top) and land cover (bottom) of the four nested domains. Position of the wind turbines and RADOME station (with data from (OpenStreetMap contributors, 2017) and (Faroux et al., 2013)). © OpenStreetMap contributors, https://www.openstreetmap.org/copyright

2.1 Wind farm : *Ensemble Éolien Catalan*

The wind farm for the study was selected based on three main criteria: its location in France, which allows the use of the AROME model as atmospheric forcing, the presence of a sufficiently large number of closely spaced turbines to investigate inter-turbine interactions and its location withing vineyards agricultural landscapes. We selected the *Ensemble Éolien Catalan* wind farm, located at the West of Perpignan in South of France. This wind farm offers several other features that make it

https://doi.org/10.5194/wes-2026-84
Preprint. Discussion started: 20 May 2026
© Author(s) 2026. CC BY 4.0 License.



eawe european academy of wind energy
Open Access WIND ENERGY SCIENCE DISCUSSIONS

particularly suitable for our study: the proximity of a RADOME meteorological station (Tardieu and Leroy, 2003) to validate the simulated atmosphere and the combined influence of the Mediterranean Sea and the Pyrenees on meteorology dynamics.

The Catalan wind farm consists of 35 turbines Vestas V80 (2 MW) and Vestas V90 (3 MW), resulting in a total installed capacity of 96 MW. The turbines are arranged approximately in four east-north-east oriented rows, forming a rectangular layout of about 5 km in length and 2 km in width (farm layout in Fig. 1). The orientation of the rows is consistent with the prevailing regional winds, which predominantly blow from the north-north-west direction.

The area surrounding the Catalan wind farm, is characterized by a complex landscape that combines coastal, mountainous, and agricultural features. To the east and southeast we find the proximity of the Mediterranean Sea. To the north and west, the terrain rises gradually toward the Corbières and Pyrénées mountain, which are predominantly covered by forested and shrubland areas, creating complex orographic effects. The immediate vicinity of the Catalan wind farm is mostly occupied by vineyards (purple in Fig. 1) with smaller patches of cereal crops and orchards. Further away, particularly toward the mountains, the landscape includes forest, Mediterranean scrubland, and scattered rural villages. This combination of orography, vegetation types, and proximity to the sea makes the region particularly suitable for studying wind farm-atmosphere interactions under realistic, heterogeneous conditions and local wind effects.

2.2 Case study : night of the 7–8 april 2021

As reported in the literature, wind-turbine-induced meteorological variations are more pronounced under strongly stratified and stable atmospheric conditions. These situations also correspond to cases where wind turbine wake extend longer, enhancing interactions between turbines within the wind farm. To investigate such situation, we focus on the night of April 7–8, 2021, during which a strong near-surface cooling event occurred across all France, leading to nocturnal frost (Fig. 2). Minimum temperatures close to the ground (50 cm) reached values down to -8 °C, marking one of the most severe spring frost events in recent years. According to the FNSEA (French National Federation of Farmers' Unions), this episode destroyed up to one-third of the national vineyard production, corresponding to an estimated economic loss of nearly 2 billion euros. In the Languedoc-Roussillon region, where the Catalan wind farm is located, losses reached approximately 70 %, with local minima down to -5.5 °C reported by the southern branch of the AOC Federation.

These extreme temperature conditions resulted from the synoptic situation prevailing at the beginning of April 2021 in Europe, characterized by a persistent anticyclone positioned South of Iceland combined with a low-pressure system over the Iberian Peninsula. This situation generated clear skies and dry air over most of France, creating favorable conditions for intense radiative cooling during nighttime. Additionally, an intrusion of cold and dry polar air affected France during few days, as reported by Météo-France in its April 2021 climate bulletin (Lemoine and Pineaud, 2021). These combined conditions resulted in cold nights, with temperatures well below seasonal averages and several new cold records across the country.

https://doi.org/10.5194/wes-2026-84
Preprint. Discussion started: 20 May 2026
© Author(s) 2026. CC BY 4.0 License.



eawe european academy of wind energy
Open Access WIND ENERGY SCIENCE DISCUSSIONS

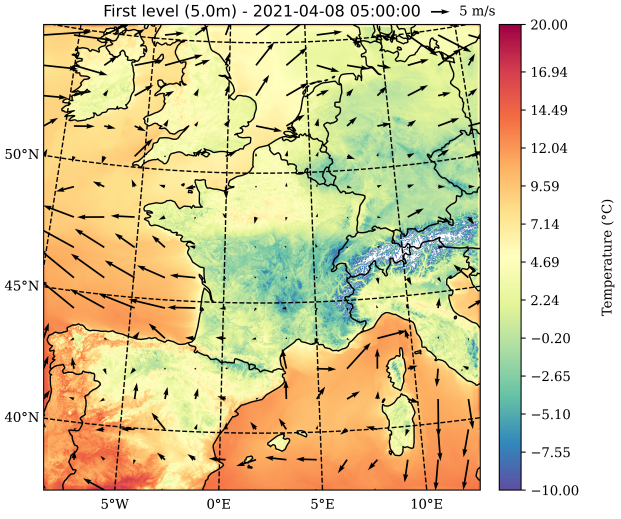


Figure 2. Temperature the 8 April 2021 at 05:00 for the first level of AROME (5 m) : negative near ground temperatures affected nearly two-thirds of southern France during that night.

3 Methods

This section describes the numerical framework used in this study. First, the multi-scale modelling setup and the atmospheric model configuration are presented. The atmospheric and surface parameterizations used to represent physical processes and land-atmosphere interactions in the different domains, as well as the associated datasets, are then described. Finally, the parameterization and configuration of the wind turbines model is detailed.

3.1 Multi-scale setup

Meso-NH is a non-hydrostatic and anelastic research atmospheric model developed by the Centre National de Recherche Météorologique (CNRM - CNRS/Météo France) and the Laboratoire d'Aérologie (LAERO - UPS/CNRS) (Lac et al., 2018). In this work, Meso-NH v5.7.1 is used to simulate the atmosphere from mesoscale to metric scales. The objective of the numerical setup is to dynamically downscale atmospheric conditions from the French operational numerical weather prediction model AROME to resolutions compatible with the wind turbine actuator parameterization.

To achieve this, a numerical setup with four nested domains is used (illustrated in Fig. 1). Their characteristics are provided in Table 1. The configuration is divided into two successive offline coupled simulations. The first simulation, referred to as the large-scale, includes domains D1 and D2, which are two-way nested and forced hourly at the lateral boundaries of domain D1 by AROME analyses. These analyses have a horizontal resolution of 1.3 km and 90 vertical levels. The large-scale simulation is run for 33h and allows the flow to be downscaled to a horizontal resolution of 125 m. Five-minute outputs from this simulation are then used to initialize and force the second simulation, referred to as the small-scale, which includes domains D3 and D4.

https://doi.org/10.5194/wes-2026-84
Preprint. Discussion started: 20 May 2026
© Author(s) 2026. CC BY 4.0 License.



eawe european academy of wind energy
Open Access WIND ENERGY SCIENCE DISCUSSIONS

This separation between large-scale and small-scale simulation is motivated both by computational cost considerations and by the fact that Meso-NH does not allow vertical grid refinement between directly nested domains. This approach makes it possible to refine the vertical resolution only in the small-scale simulation, where the wind turbines are located. The domain D4 with a horizontal resolution of 5 m and and a vertical resolution of 4 m encompasses the Catalan wind farm area. Its horizontal size was chosen to ensure that turbulence is fully developed before the flow reaches the wind turbines and the meteorological tower locations.

The complex topography and the large resolution jump prevent domain D4 from being directly initialized and run from output of domain D2. Therefore, the small-scale simulation is first run using domain D3 alone for a 45-minute spin-up period. The resulting atmosphere is then used to initialize domain D4. Finally, domains D3 and D4 are run in a one-way nested configuration for a total duration of 55 minutes. To allow the small-scale atmospheric flow and turbine wakes to develop, the simulation includes a 25-minute spin-up period, followed by a 30-minute averaging period.

Simulation	Domain	$N_x \times N_y \times N_z$	$\Delta x = \Delta y$ [m]	$\Delta z_{0\mathrm{m}}$ [m]	$\Delta z_{300\mathrm{m}}$ [m]	L_z [km]	Δt [s]	WT
Large-scale	D1	$500 \times 500 \times 70$	625	4	$\sim$50	18	2.00	-
	D2	$500 \times 500 \times 70$	125	4	$\sim$50	18	0.25	-
Small-scale	D3	$1000 \times 1000 \times 152$	25	4	4	2.6	0.10	-
	D4	$1500 \times 1080 \times 152$	5	4	4	2.6	0.10	ADR

Table 1. Domain dimensions of the numerical setup.

3.2 Atmospheric parameterizations

In this work, the choice is made to solve the pseudo-compressible system of equations as defined by (Durran, 1989). The turbulence is treated with a tree-dimensional scheme (Cuxart et al., 2000) and closed with a mixing length as defined by Deardorff in 1980 (Honnert et al., 2021). Deep and shallow convection are explicitly resolved at the exeption of domain D1 in which the Eddy-Diffusivity-Kain-Fritsch parameterization is used for shallow convection (Pergaud et al., 2009). Wind advection is treated with the explicit Runge-Kutta centered 4^{th} order scheme for time integration and a 4^{th} order centered spatial scheme for space. Additional physical parameterizations include the ECRAD radiation scheme (Hogan and Bozzo, 2018) and a subgrid cloud model and the ICE3 microphysics scheme (Caniaux et al., 1994; Pinty and Jabouille, 1998) for water phase transformations.

3.3 Surface parameterizations

An online coupling with the SURFEX v9.0 surface transfer model (Masson et al., 2013) is employed to finely model surface exchange with the atmosphere. Soil and vegetation effects are captured through the explicit multilayer model ISBA-DF (Boone et al., 2000; Decharme et al., 2011) which solves the heat and mass transfer equations in the soil with 14 vertical soil layers. Urban effects are modeled using the TEB model (Masson, 2000). Usually the SURFEX model is used with the global 1 km

https://doi.org/10.5194/wes-2026-84
Preprint. Discussion started: 20 May 2026
© Author(s) 2026. CC BY 4.0 License.



eawe european academy of wind energy
Open Access WIND ENERGY SCIENCE DISCUSSIONS

resolution ECOCLIMAP-II surface database (Faroux et al., 2013). However in our case its level of detail is insufficient for the resolution of domains D2, D3, and D4, as well as for accurate representation of the Catalan wind farm area. Therefore, a high resolution surface database was created by extracting surface data from OpenStreetMap (OpenStreetMap contributors, 2017) using the Geoclimate tool (Bocher et al., 2021). The surface classes provided in OpenStreetMap were then manually convert as cover classes as defined in ECOCLIMAP-II and given as input to SURFEX (Fig. 1). While this method depends on somewhat arbitrary reclassification choices, it nevertheless provides a surface database that captures the fine-scale specification of the wind farm environment with a level of detail that does not exist in standard datasets, particularly at resolutions of 5m.

However, transferring soil initial conditions from the force restore two-layer ISBA-FR model of AROME to a 14-layer soil representation is physically challenging, especially for deep soil temperatures. A strong sensitivity of the initial soil condition to the time of initialization was also identified. Technically, a multi-day surface spin-up would have been required to properly equilibrate the ISBA-DF soil profile, but this approach is computationally expensive. Instead, a simplified initialization was adopted, in which the 14 soil layers were initialized using the mean air temperature of the first AROME level over the previous 24 hours. This method produced more realistic deep soil temperatures for April conditions and led to a nocturnal cooling closer to experimental observations (see section 4.1).

3.4 Wind turbine parameterizations

3.4.1 Actuator disk

In Meso-NH, three wind turbine wake modeling approaches have been implemented and validated. The first one is the Actuator Disk with No Rotation (ADNR), which consists in representing the wind turbine as a disk on which a thrust force is applied. Although computationally inexpensive, this approach does not account for blade rotation or detailed aerodynamic characteristics. The second one is the Actuator Line Method (ALM) (Joulin et al., 2020), which provides a detailed representation of individual blade effects and wake dynamics. This approach is however computationally very expensive, as it requires high spatial and temporal resolutions to resolve explicitly blade rotation. To overcome these limitations and provide a compromise between accuracy and computational cost, the Actuator Disk model with Rotation (ADR) has been implemented in Meso-NH since version 5.7.0 (Boumendil et al., 2024), offering a more affordable alternative while still capturing the rotational effects. As for the ALM, aerodynamic blade profiles along the span and their associated aerodynamic polars are used to compute the forces applied to the flow. These forces depend on the local incoming wind speed and on the rotational speed of each blade element. They are then applied to the atmospheric flow using a three-dimensional linear smearing method. A tip-loss correction function is also applied to avoid overestimation of loads near the blade-tip region.

As in our previous studies (Boumendil et al., 2024, 2025), a single equivalent 2 MW wind turbine is used to represent both the Vestas V80-2MW and V90-3MW turbines. This turbine is scaled while preserving its original airfoil data for the ADR model. To achieve this, the blade geometry is uniformly scaled to a rotor diameter of $D = 90$ m and the rotation speeds are adjusted to maintain an iso tip-speed ratio. Finally, the twist angle is modified to obtain, as output, thrust C_t and power C_p coefficients close to those of the Vestas.

https://doi.org/10.5194/wes-2026-84
Preprint. Discussion started: 20 May 2026
© Author(s) 2026. CC BY 4.0 License.



eawe european academy of wind energy
Open Access WIND ENERGY SCIENCE DISCUSSIONS

The turbines of the Catalan wind farm are represented by 35 ADR, each discretized using an azimuthal mesh ($N_\theta = 80$) and a radial mesh ($N_r = 46$). The spatial resolution of domain D4, in which the ADR are implemented, has been chosen to ensure at least 16 Meso-NH grid cells across the rotor diameter. The center of each actuator disk is positioned at a height of 80 m above the local terrain, accounting for the individual elevation of each turbine. The effects of the nacelle and the tower are not modeled.

3.4.2 Controlling

As in a real wind farm, each ADR experiences different wind speeds and directions, due both to atmospheric variability and to wake interactions. Consequently, the operational parameters of each turbine are controlled individually. Several turbine controllers are available in Meso-NH/EOL. It allows the control of rotor speed, blade pitch angle, and nacelle yaw orientation. For each of these parameters, one or several control strategies are available.

In this study, the rotor rotational speed and blade pitch angle are computed using a simple control strategy based on lookup tables. The reference incoming wind speed U_∞ for each turbine is estimated as a 1-minute average over a disk located one rotor diameter upstream of the turbine. The nacelle yaw angle is controlled dynamically. Similarly, the mean wind direction is evaluated every minute on a disk located $1D$ upstream of each turbine. At this interval, each ADR then progressively rotates its nacelle angle at each model time step to align with the simulated wind direction.

4 Validation and analysis of the simulation

This section presents the atmospheric conditions simulated before the activation of the ADR. First, the simulated atmospheric fields are evaluated against available observations. Then the large-scale atmospheric situation over the Languedoc-Roussillon region is described to provide the synoptic context of the event. Finally the analysis focuses on the atmospheric conditions over the wind farm area in the small-scale simulation, with particular attention to the horizontal and vertical structures of the flow that will interact with the turbines.

4.1 Comparison against the observations

The 5-minute averaged time series of some meteorological variables from the large and small-scale simulations are validated using measurements from the meteorological station located at the Perpignan airport (Fig. 3). This station is part of the operational surface observation network of Météo-France, known as RADOME (Tardieu and Leroy, 2003) (see position in domain D3 in Fig. 1). Consequently, only a limited set of meteorological variables is available, measured at 2 m and 10 m above ground level. Vertical atmospheric profiles derived from domain D2 are also shown in Fig. 4.

The comparison between experimental measurements and simulations shows overall good agreement. The 10 m wind speed and direction closely match those observed at the RADOME station (Fig. 3a-b). During the daytime, the wind exhibits characteristics typical of an unstable atmospheric boundary layer. After sunset, wind speeds decrease and the flow structure becomes more complex (Fig. 4a-b), reflecting the influence of locally driven winds induce by the complex topography. During the day

https://doi.org/10.5194/wes-2026-84
Preprint. Discussion started: 20 May 2026
© Author(s) 2026. CC BY 4.0 License.

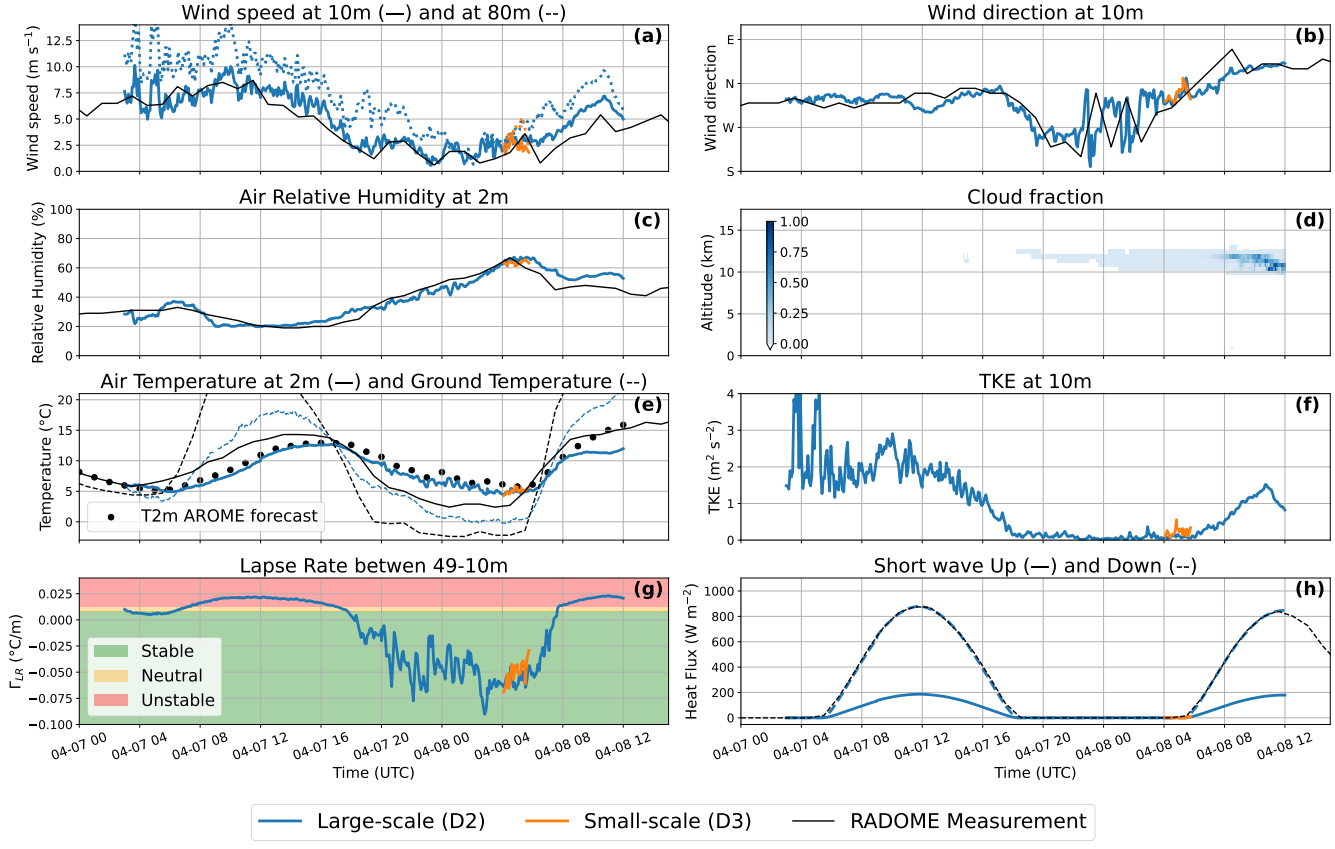


Figure 3. 5-min averaged time series of (a) Wind speed, (b) Wind direction, (c) Relative Humidity , (d) Cloud fraction (e) Air and ground Temperature, (f) TKE , (g) Static Stability between 49 and 10 m, (h) Downward and Upward Short Wave Heat Flux at the Perpignan airport RADOME station and in the domains D2 and D4 between the 7–8 April 2021.

on 7 April, the air remains relatively dry, with near-surface relative humidity around 25 % (Fig. 3c). Later, changes in wind direction associated with fronts arriving from the sea bring a marked increase in atmospheric moisture. High-altitude clouds, likely cirrus, appear after sunset at altitudes between 10 and 15 km (Fig. 3d). The temporal evolution of TKE at 10 m follows a clear diurnal cycle (Fig. 3f). Daytime values on 7 April are relatively high due to enhanced convective activity and strong near-surface winds. After sunset, the TKE progressively decreases as wind speeds weaken and the atmosphere stabilizes, resulting in low turbulence levels throughout the night. With the return of daytime heating on 8 April, the TKE increases again as thermal mixing redevelops, although values remain lower than those observed the previous day.

The main difference between the experimental measurements and the simulation lies in the nocturnal cooling (solide line in Fig. 3e). A warm bias of approximately 2–3 °C is observed for the 2 m air temperature, as well as for the surface temperature (dotted line in Fig. 3e). This warm bias is also present in the AROME forecast for the same period (black dot in Fig. 3e). Given that Meso-NH is forced by AROME and that both models share similar physical parameterizations, this result is coher-

https://doi.org/10.5194/wes-2026-84
Preprint. Discussion started: 20 May 2026
© Author(s) 2026. CC BY 4.0 License.

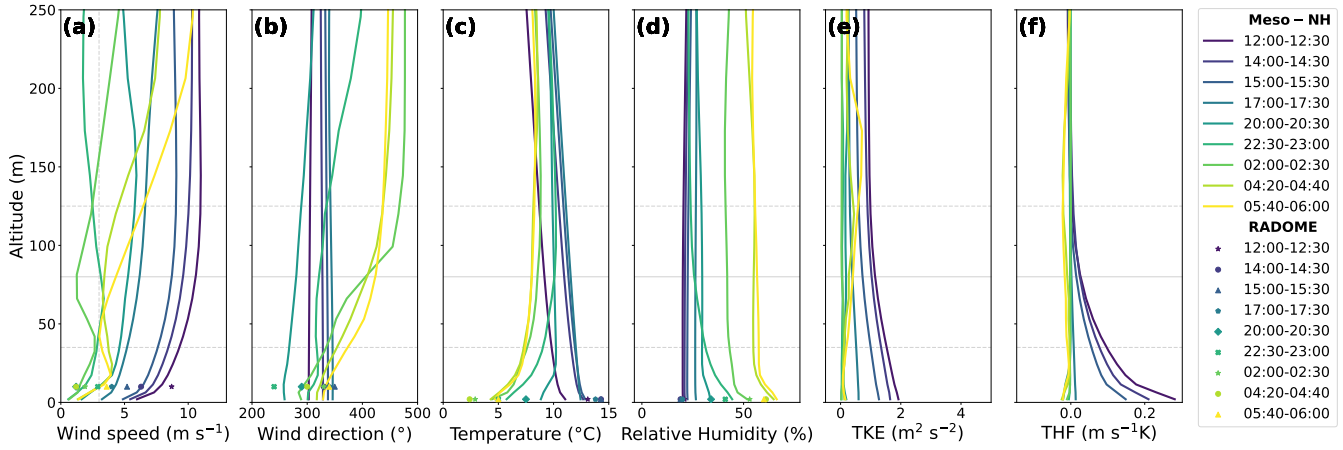


Figure 4. 30-min averaged vertical profiles of (a) Wind speed, (b) Wind direction, (c) Temperature, (d) Relative Humidity (e) TKE, (f) Turbulent heat flux, at the Perpignan RADOME station in the Domain D2. The wind turbine hub and rotor dimension are represented by solid and dashed grey lines.

ent. However, one could have expected that the higher resolution of the Meso-NH setup and surface data, combined with the forcing by AROME analysis, would have reduced this warm bias. Several sensitivity experiments were conducted, including variations in the mixing-length formulation, soil model equations, soil temperature initialization, and atmosphere-surface coupling coefficients. The results show a sensitivity of nocturnal cooling to these parameters; however, no combination was able to reproduce the observed cooling at the measurement site (not shown). Overall, the warm bias appears to be primarily linked to soil temperature overestimation, themselves resulting from the initialization of subsurface temperatures in the ISBA-DF model. The revised methodology used to compute soil temperature, described in section 3.3, improved nocturnal cooling but did not fully remove the bias. This highlights the complexity of modeling surface-atmosphere interactions and reproducing specific meteorological situations, even at high spatial resolutions (Kale et al., 2023; Bakhoday-Paskyabi et al., 2022).

Furthermore, this validation remains limited due to the availability of only a single near-surface measurement point, and the lack of validation at rotor height or for turbulence quantities such as TKE. Nevertheless, the atmospheric conditions simulated here are consistent with the primary objective of this study : to reproduce a stable and stratified boundary layer to investigate its interaction with wind turbine and surface properties. Wu and Archer (2021); Boumendil et al. (2024, 2025) suggest that under such atmospheric condition pronounced turbine-induced temperature perturbations can be expected.

4.2 Analysis of the large scale atmospheric condition around the wind farm

Horizontal cross-sections of wind speed at hub height (80 m above ground level) in domains D1 and D2 are shown in Figure 5 (a video is also available at https://doi.org/10.5446/73018). During the morning and early afternoon of 7 April, strong winds blow from the Languedoc coast toward the Mediterranean Sea (Fig. 5a). After sunset, the associated nocturnal cooling leads to a marked decrease in wind speed in the Perpignan area (Fig. 5b). Over the Mediterranean Sea, a mesoscale frontal zone

https://doi.org/10.5194/wes-2026-84
Preprint. Discussion started: 20 May 2026
© Author(s) 2026. CC BY 4.0 License.

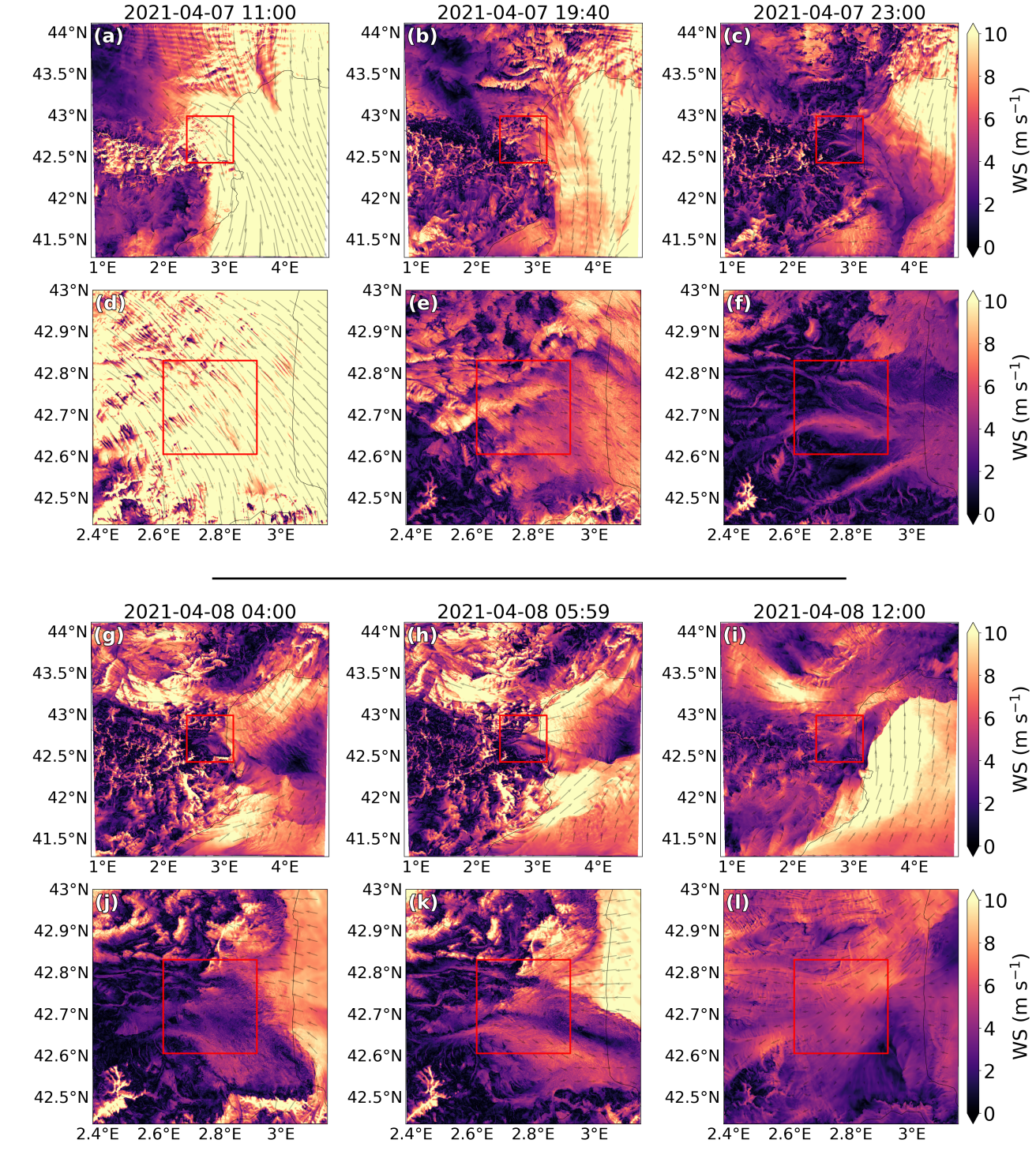


Figure 5. Vertical cross-sections of wind speed at 80 m above ground level from the large-scale simulation. The upper line of each panel shows domain D1 (a,b,c,g,h,i) and the lower line shows domain D2 (d,e,f,j,k,l). The red box indicates the extent of the son domain.

https://doi.org/10.5194/wes-2026-84
Preprint. Discussion started: 20 May 2026
© Author(s) 2026. CC BY 4.0 License.



eawe european academy of wind energy
Open Access WIND ENERGY SCIENCE DISCUSSIONS

develops as a result of the convergence of three air masses, further reinforcing the weak-wind conditions over Perpignan (Fig. 5c). Under these conditions, the local flow becomes primarily controlled by orography, with slope and valley winds dominating the circulation (Fig. 5f). Between 20:00 and 04:00, wind speeds remain around 3–4 ms^{-1}, which is close to the cut-in wind speed of the turbines.

After 04:00, the frontal system progressively shifts over the Mediterranean. A strong marine flow then penetrates inland, guided by the Albères massif South of Perpignan. A recirculation pattern develops, leading to the formation of a mesoscale vortex over the Perpignan area (Fig. 5j–k). As a consequence, toward the end of the night, the wind farm is exposed to easterly to northeasterly winds, which enhance wake interactions along the turbine rows (see wind farm layout in Fig. 1). This late-night period, characterized by a strong nocturnal cooling, a highly stratified atmosphere, and wind speeds sufficient for turbine operation, represents a particularly interesting case for the present study.

4.3 Analysis of the small scale atmospheric condition at the wind farm area

Vertical cross-sections of domain D3 at 04:50 are shown in Fig. 6 (see segment AB on the horizontal cross-sections). The wind turbine actuator disk model is not activated at this step, however, turbine locations are indicated to provide a clearer view of the spatial scales and extent of the wind farm. A pronounced horizontal and vertical heterogeneity is visible in the different meteorological fields. In the vertical cross-sections, an air mass originating from the Mediterranean Sea enters the domain from the right (Fig. 6b). This air mass is characterized by higher wind speeds, warmer temperatures, and greater moisture content compared to the continental air. Because the land surface is cooler, the warmer marine air mass tends to overrun the cold and dry air near the surface (see bottom left of Fig. 6h and j). This configuration leads to global positive vertical velocities (Fig. 6f) and the development of strong wind shear at the interface between the two air masses. Such shear conditions are favorable to Kelvin-Helmholtz instabilities, which are noticeable on the left bottom of vertical cross section by the presence of vortical structures in the wind and temperature fields (Fig. 6b and h), as well as by enhanced turbulence and alternating ascending and descending air motions (Fig. 6d and f).

At the surface, temperature also exhibits strong spatial heterogeneity: hilltops are relatively warmer while valleys remain cooler, a pattern typical of thermally driven slope and valley circulations under stable nighttime conditions (Fig. 6g). Near-surface winds follow the slope orientation and are partially decoupled from the flow at hub height, indicating the presence of a stratified boundary layer regime. Surface relative humidity (Fig. 6i) further highlights the contrast between the two air masses: a moist marine air mass advected from the sea and a drier air mass descending from the mountains.

5 Results : Interaction between the atmosphere and the wind farm

The meteorological variations, denoted Δ, are computed as the difference between two identical small scale simulations performed with actuator denoted as ADR and without actuator denoted as Ref. This approach allows to isolate the atmospheric perturbations directly attributable to turbine wakes from those that would have occurred independently of the presence of the wind farm. Such a methodology constitutes a major advantage of numerical simulations over experimental measurements,

https://doi.org/10.5194/wes-2026-84
Preprint. Discussion started: 20 May 2026
© Author(s) 2026. CC BY 4.0 License.

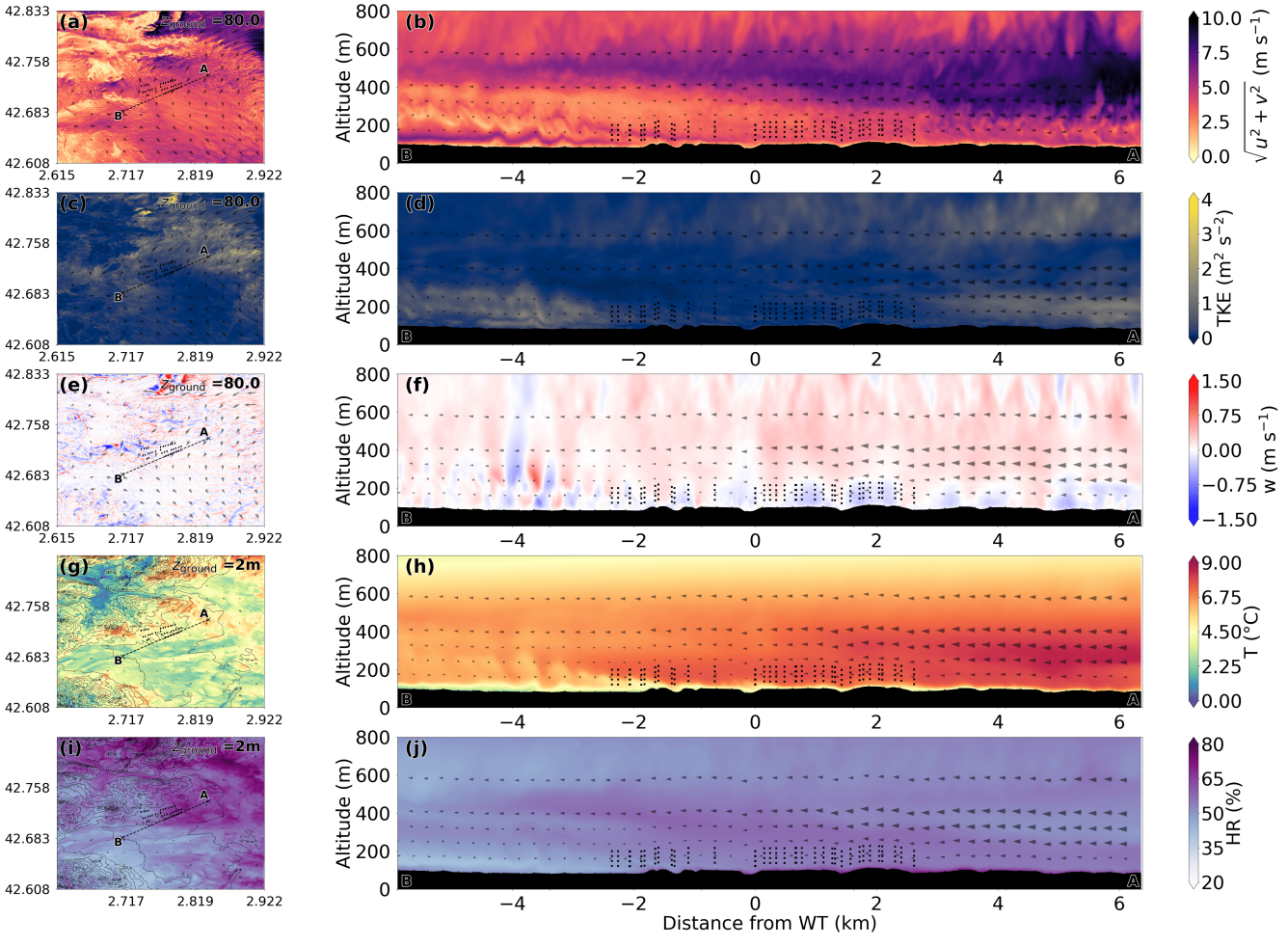


Figure 6. Domain D3 at 04:50 the 8 april 2021. First column : horizontal cross-sections (at hub height 80 m or at 2 m above the ground), second column : vertical cross-sections along the segment AB. The positions of the wind turbines, which are not activated in this domain, are represented by dotted black lines. The terrain on the vertical cross-sections is represented in black and altitude zero is equal to sea level.

for which distinguishing turbine-induced effects from natural atmospheric variability is particularly challenging and require statistical methodology (Wu and Archer, 2021; Rajewski et al., 2016).

The large-scale atmospheric conditions generated in the domain D1 propagate down to domain D4, where they interact with the wind turbines. The simulations in domain D4 are run between 04:50 and 05:45 (see orange line on Figure 3). Vertical atmospheric profiles at the center of domain D4 from the Ref simulation are available in appendix Fig. A1. The analysis focuses on the last half-hour before sunrise, when the near-surface air layer reaches its lowest temperatures and the risk of frost over the vineyards is the greatest. At this time of the night, hub-height wind speeds also increase sufficiently for the turbines to operate (see orange dotted line on Fig. 3a).

https://doi.org/10.5194/wes-2026-84
Preprint. Discussion started: 20 May 2026
© Author(s) 2026. CC BY 4.0 License.

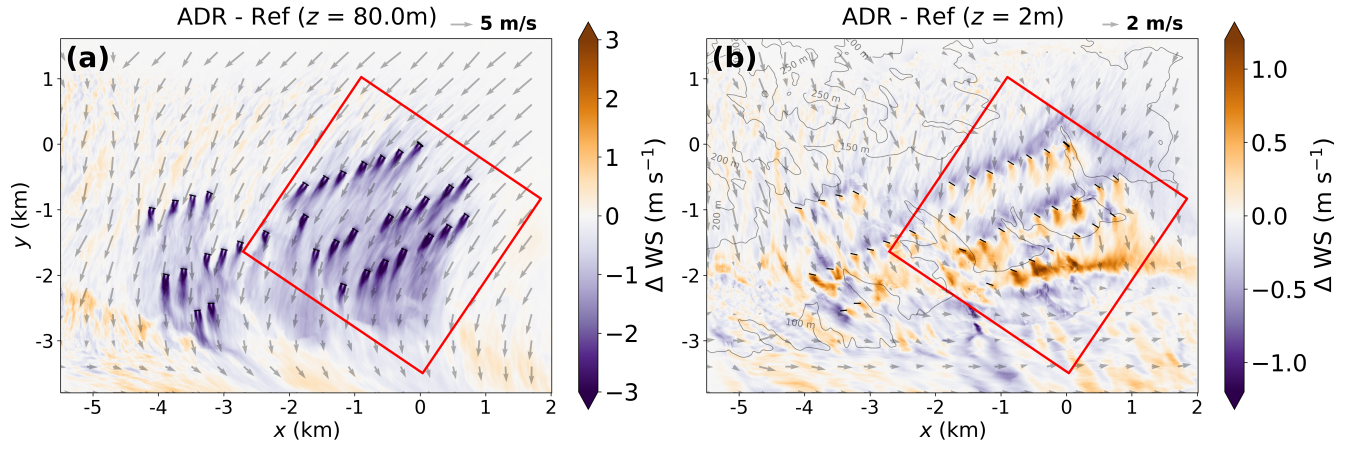


Figure 7. Mean horizontal cross-sections between 05:15 and 05:45 of wind speed deficit (ADR - Ref) at (a) 80 m and (b) 2 m . Wind turbine positions are indicated by black segments. Wind speed and direction are represented by grey arrows. Terrain contours are shown in grey.

5.1 Strong wind direction veer effect between hub height and near surface level

The wind regime during the end of the night over the Perpignan wind farm is dominated by a mesoscale vortex, due to sea and mountain flows interactions. At the hub height, the wind blows from the north-northwest and exhibits a counterclockwise deflection between the upstream and downstream parts of the farm. As a result, the velocity deficit reveals wake directions that can differ by up to 45° within the wind farm, despite its relatively compact layout (Fig. 7a). Horizontally, wake expansion is enhanced by the gradual turning of the wind direction across the farm. Velocity deficits generated by upstream turbines impact downstream rows. Power output is maximal for turbines located along the outer edges of the farm, unaffected by upstream wakes, whereas turbines within the interior can produce around twice less power (Fig. 8). This contrast is further reinforced by the fact that the background wind speed downstream the farm is weaker even in the absence of upstream wake effects (Appendix Fig. B1a).

A localized acceleration zone is visible near the ground beneath each rotor (Fig. 7b). Such sub-rotor accelerations have been previously reported in idealized LES studies (Xie and Archer, 2017; Wu et al., 2023), particularly under stable atmospheric conditions. This effect is attributed to turbine-induced pressure field adjustments that channel the flow beneath the rotor, producing a Venturi acceleration. The phenomenon is enhanced under stable stratification, where vertical motions that would otherwise allow the flow to pass the obstacle are strongly suppressed (Xie and Archer, 2017). At the wind farm scale, flow acceleration is also observed above the farm (Appendix Fig. B1e) and along its lateral edges (Fig. 7a). These positive wind speed anomalies arise from the same mechanism as the sub-rotor acceleration but acting at the scale of the farm. The farm behaves as a obstacle that locally modifies the atmospheric circulation, forcing the flow to accelerate around and above the farm to ensure mass conservation. Similar large-scale acceleration patterns have been reported in offshore wind farm simulations using the Fitch wind farm parameterization (Quint et al., 2025).

https://doi.org/10.5194/wes-2026-84
Preprint. Discussion started: 20 May 2026
© Author(s) 2026. CC BY 4.0 License.

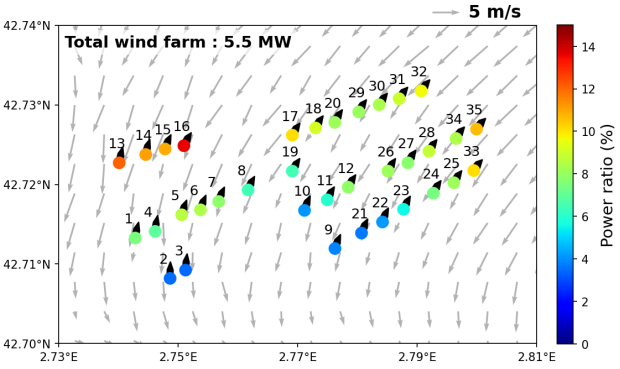


Figure 8. Mean wind turbine power ratio between 05:15 and 05:45. The nacelle orientation is indicated by a small black arrow on each turbine

5.2 Near ground meteorological variations induce by individual wind turbines and the farm

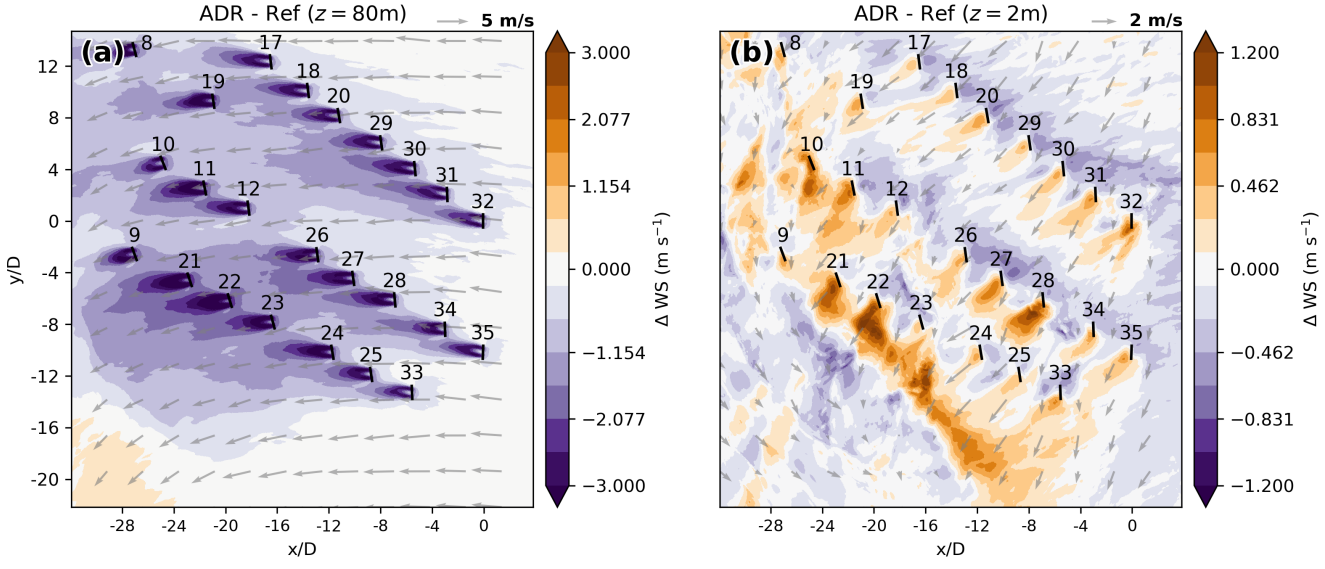


Figure 9. Subdomain horizontal cross-sections of wind speed deficit (ADR - Ref) at 80 m (a) and 2 m (b) above ground level. Wind turbine positions are indicated by black segments. Wind speed and direction are represented by grey arrows.

330 We now focus on the near-surface meteorological variations induced by the wind turbines. In order to simplify the analysis, we restrict the study to the eastern part of the wind farm, where the turbine density is highest and where the largest perturbations are observed. The study domain is therefore limited to the red rectangle in Fig. 7. The subdomain origin is centered and aligned with the wind direction at hub height of the most upstream turbine in the farm : wind turbine number 32.

https://doi.org/10.5194/wes-2026-84
Preprint. Discussion started: 20 May 2026
© Author(s) 2026. CC BY 4.0 License.

Figure 9 shows the wind speed deficit induced by the turbines within the subdomain at 80 and 2 m above ground level. A strong difference in wind direction is observed between hub height and the near-surface layer, with deviations approaching 30–50°. At 80 m, the wake structures exhibit the typical downstream spreading, while an upstream induction zone is visible in front of each turbine as well as a larger-scale induction zone associated with each turbine row. Near the ground, wind speed variations are also present. Although their magnitude is smaller than at hub height, they represent relatively large perturbations when compared to the weak background wind speeds close to the surface.

Near the ground a reduction in wind speed is observed upstream of turbine rows, while beneath the rotor localized acceleration occurs, consistent with the sub-rotor acceleration mechanism described in Section 5.1. In addition, downstream of the last turbine row, a region characterized by alternating positive and negative wind anomalies is visible. This region coincides with a convergence zone between two air masses with different flow directions (see converging arrows in Fig. 9b) and distinct temperatures (see the next paragraph and Fig. 10a). These wind anomalies therefore appear to result primarily from a modification of the position of the katabatic flow and the convergence zone, rather than from the individual influence of the turbines.

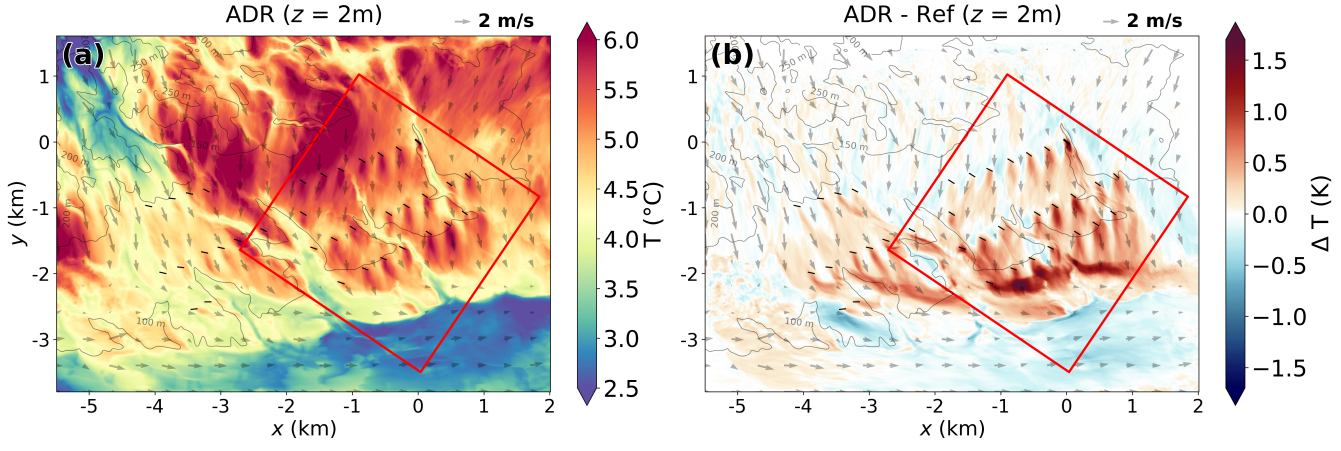


Figure 10. 2 m mean horizontal cross-sections of (a) temperature (ADR) and (b) temperature variation (ADR - Ref) between 05:15 and 05:45. Wind turbine positions are indicated by black segments. Wind speed and direction are represented by grey arrows. Terrain contours are shown in grey

The 2 m air temperature T and temperature variation ΔT field are plotted in Fig. 10. As for the wind speed deficit, we restrict our study area to the red rectangle. The subdomain temperature in the Ref and ADR simulation is plotted in Fig. 11 while the subdomain temperature variation ΔT is plotted in Fig. 12a. The temperature field exhibits strong spatial variability as cold air accumulates within valley floor, while terrain elevations remain comparatively warmer. A katabatic flow is visible in the valley located downstream of the wind farm (blue/yellow air mass in Fig. 10a and 11), producing a front between the different local flow.

In the ADR simulation (Fig. 11c), localized warming zones appear downstream of the turbines and are advected by the near-surface flow. The temperature averaged along the x-axis (Fig. 11b) shows a difference of nearly 2 °C between the upstream

https://doi.org/10.5194/wes-2026-84
Preprint. Discussion started: 20 May 2026
© Author(s) 2026. CC BY 4.0 License.

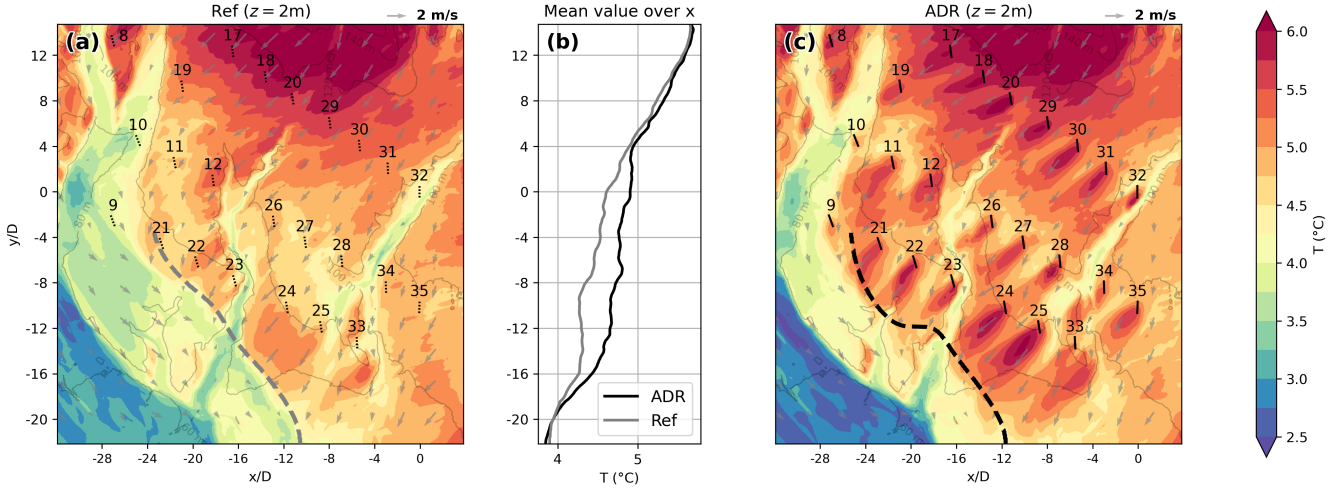


Figure 11. Subdomain 2 m horizontal cross-sections of air temperature for the (a) Ref and (c) ADR simulation. Wind turbine positions are indicated by black segments. Wind speed and direction are represented by grey arrows. Terrain contours are shown in grey. The maximum convergence line of the 2 m wind field, corresponding to the boundary between the two air masses, is indicated by a dotted line. (b) 2 m temperature averaged along the x-axis for the ADR and Ref simulations

and downstream parts of the farm in both simulations. Therefore the contribution of the wind farm has to be evaluated by comparing the two curves. The difference is limited to its immediate vicinity of the farm and shows a mean warming anomaly of up to 0.4 °C.

The maximum convergence of the 2 m wind field is indicated by the dotted line in Fig. 11. This line marks the position of the katabatic front separating the two interacting air masses. The comparison of its position in simulations Ref and ADR (Fig. 12) shows that the presence of the wind farm shifts this convergence zone southward by approximately 100–400 m downstream of the farm. As a result, strong temperature variations are observed along this frontal zone, reflecting the different thermodynamic properties of the interacting air masses.

Temperature variations ΔT (Fig. 12a) confirm the localized warming patterns downstream wind turbines. However, they also highlight the presence of cooling anomalies of around 0.2 °C in some areas surrounding the wind farm.

The strongest warming beneath the rotors occurs for turbines located within valleys where cold air tends to accumulate (turbine 32, 10 or 9). In these locations, turbine-induced mixing interacts with stronger temperature inversions, bringing warmer air from aloft down toward the surface and thus generating stronger anomalies. For example, a temperature increase of up to 1.6 °C is observed downstream of wind turbine 32. Another region where strong meteorological variations are observed is along the katabatic flown. In this area, a pronounced warming trail reaching nearly 2 °C is visible (Fig. 12b). These temperature anomalies are therefore primarily associated with the displacement of the convergence zone induced by the wind farm rather than with the direct contribution of the third turbine row.

https://doi.org/10.5194/wes-2026-84
Preprint. Discussion started: 20 May 2026
© Author(s) 2026. CC BY 4.0 License.

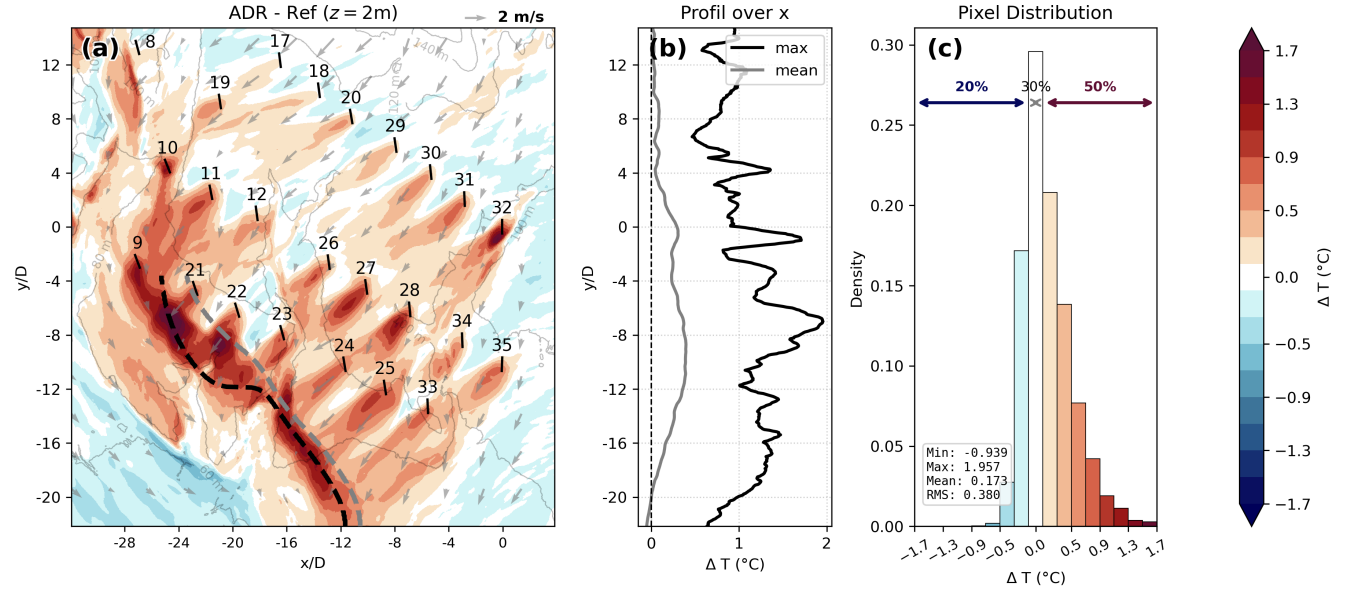


Figure 12. (a) Subdomain mean horizontal cross-section of the 2 m temperature variation (ADR - Ref) between 05:15 and 05:45. (b) Maximum and mean 2 m temperature variation along the x-axis. (c) Histogram of temperature variations within the subdomain.

The histogram of temperature variations (Fig. 12c) indicates that, although both warming and cooling occur within the subdomain, the amplitude of warming anomalies is larger than that of cooling anomalies. This suggests that under these conditions turbine-induced mixing tends to increase near-surface temperatures downstream of the wind farm, while modifications of the flow field around the farm tend to slightly cool the surrounding regions. These statistics should, however, be interpreted with caution, as they strongly depend on the arbitrary choice of the study subdomain boundaries.

5.3 Differentiate effects on ground temperature across the wind farm

Figure 13 shows the ground temperature variation induce by the wind turbine at the first level (0.1mm) of the SURFEX/ISBA surface model (rivers and lakes are excluded). Warming patterns are visible starting from the rotor location of each turbine, corresponding to the near-surface air temperature increases previously identified. In contrast, cooling anomalies appear upstream of turbine rows, in regions where wind speed is reduced due to the blockage effect. These results suggest that ground temperature variations result from a combination of changes in wind speed and near-surface air temperature. This interpretation is consistent with the formulation of the sensible heat flux from the surface model, which depends on both the surface-atmosphere temperature difference and the turbulent exchange driven by wind speed near the surface.

https://doi.org/10.5194/wes-2026-84
Preprint. Discussion started: 20 May 2026
© Author(s) 2026. CC BY 4.0 License.

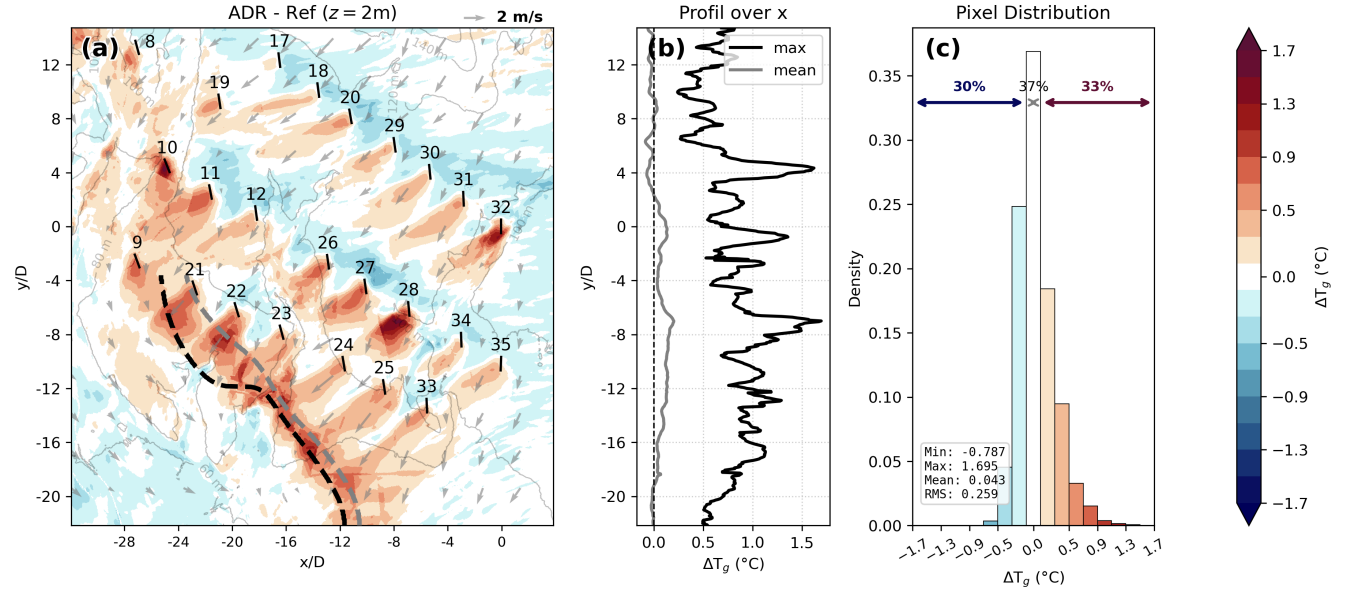


Figure 13. (a) Subdomain horizontal cross-section of the ground temperature difference at 05:45 (end of the simulation) between ADR and Ref. (b) Maximum and mean ground temperature variation along the x-axis. (c) Histogram of ground temperature variations within the subdomain.

6 Discussion

6.1 Physical processes controlling turbine-atmosphere interactions

The results highlight the importance of local atmospheric flows when investigating wind farm-atmosphere interactions in complex environments. In the present case, both the complex terrain and the stable and strongly stratified atmospheric conditions play a key role in shaping the flow. These results therefore underline the relevance of realistic multiscale simulations to investigate such phenomena, as they allow the representation of both mesoscale atmospheric structures and local flow modifications induced by topography and wind turbines.

The simulations reveal a strong heterogeneity of meteorological conditions across the domain. Significant spatial variabilities are observed in both wind speed and wind direction, horizontally as well as vertically. This heterogeneity becomes even more pronounced near the surface. In particular, local katabatic flows lead to the interaction of air masses with very different properties. As a result, the near-surface atmosphere is already highly intricate before any interaction with the wind turbines occurs.

Within this already complex flow, wind turbines introduce additional perturbations that further modify the atmospheric circulation. Under the stable and strongly stratified conditions of our case, turbines contribute to vertical mixing through two main mechanisms. First, organized advection at the rotor level as the rotating blades induce vertical motions. Second, turbulent

https://doi.org/10.5194/wes-2026-84
Preprint. Discussion started: 20 May 2026
© Author(s) 2026. CC BY 4.0 License.

motions generated in the wake propagate these perturbations through turbulent transport, allowing temperature and momentum anomalies to reach the near-surface layer.

At the wind turbine scale, the alignment of turbines in rows causes an obstacle to the flow. This is visible through the induction zones that extend upstream of each turbine row and of the Venturi acceleration below the rotor. A similar effect is observed at the scale of the entire wind farm, which locally modifies the atmospheric circulation around it. Acceleration zones appear along the lateral edges of the farm, while the position of nearby air masses is also slightly displaced. In the present case, the complex meteorological conditions and the strong stratification further amplify these effects.

The amplitude of the meteorological variations induced by each turbine appears to be strongly influenced by local topography. In particular, turbines located within valleys generate the largest perturbations, as they interact with stronger near-surface temperature inversions. These results are consistent with the experimental findings of (Wu and Archer, 2021) and the numerical results of (Boumendil et al., 2024), which highlight a strong relationship between near-surface thermal stratification and the magnitude of turbine-induced temperature variations. In contrast, the amplitude of these variations does not seem to be primarily controlled by the turbine power production (Fig. 8) nor by its spatial position within the wind farm.

Finally, by examining the 3D temperature iso-surfaces from Fig. 14, it can be observed that the warming region extends throughout the downstream area of the wind farm while progressively rising in altitude. As a result, this warming is not visible in the 2 m horizontal cross-sections shown in Fig. 12a.

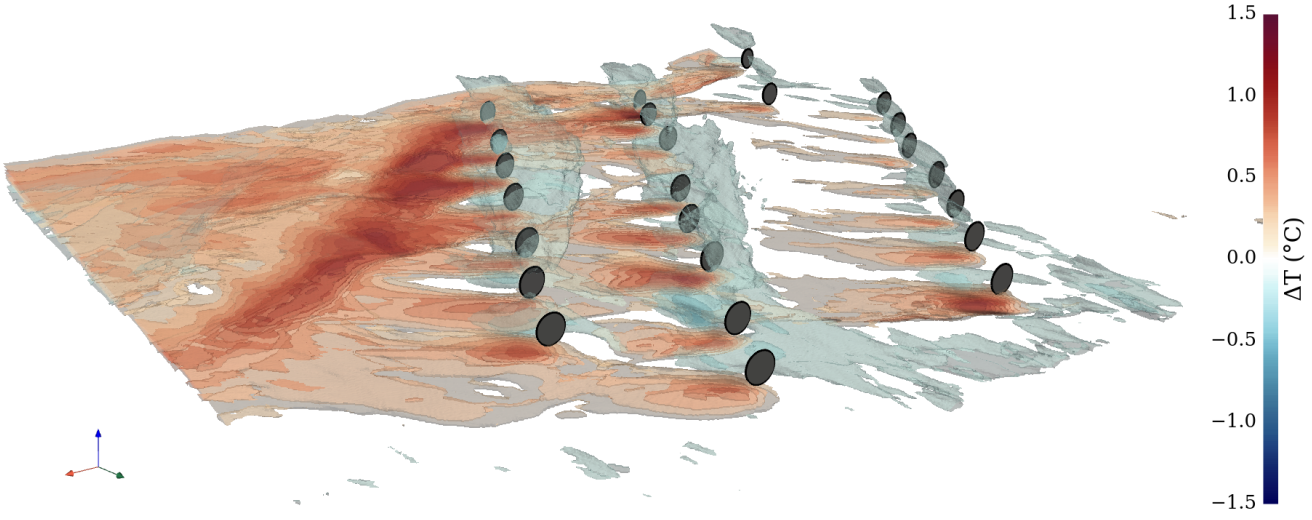


Figure 14. 3D iso-surface of the temperature variation in the subdomain

The atmospheric perturbations generated by the turbines also propagate to the surface through atmosphere-land coupling processes. Variations in ground temperature ranging from -0.7 to +1.6°C are observed in the first layer of the ground model.

https://doi.org/10.5194/wes-2026-84
Preprint. Discussion started: 20 May 2026
© Author(s) 2026. CC BY 4.0 License.



These variations are consistent with the combined effects of changes in near-surface air temperature and wind speed, which control the turbulent heat exchanges between the atmosphere and the surface. In regions where turbine-induced warming is advected near the surface, the ground temperature also increases, whereas upstream of turbine rows, where wind speed decreases due to blockage effects, the ground temperature tends to decrease.

6.2 Implications for vineyards and frost events

From the perspective of vineyard protection, the simulations indicate that wind turbines induce a mean near-surface warming of approximately 0.4 °C within the wind farm immediate area, with local maxima reaching up to 1.6 °C. Although these temperature increases remain relatively small, they are of the same order of magnitude as those produced by frost protection fans commonly used in vineyard (Le Cap et al., 2024). As a example the Food and Agriculture Organization of the United Nations (FAO) (Snyder and de Melo-Abreu, 2005) indicates that the 2 m temperature variation corresponds to roughly 30 % of the inversion strength between 2 m and 10 m, and recommends the use of fans when the inversion exceeds 1.5 °C and wind speeds near the ground are below 2.5 ms^{-1}. It should be noted, however, that frost protection fans rotate, providing a 360° action and operated on demand without the constraint of sufficient wind speed at hub height as wind turbines.

However, the simulations also reveal ground cooling zones and wind speed reductions in some areas surrounding the farm. According to FAO recommendations, wind plays an important role in limiting frost damage by preventing cold air stagnation near the ground. Therefore, the spatial redistribution of wind and temperature induced by the wind farm may lead to both beneficial and adverse effects depending on the local position within the vineyard landscape.

Our simulations are consistent with reports from winegrowers indicating that frost damage can vary significantly from one location to another during the same frost event. This spatial variability is also present in the simulations, which show strong heterogeneity in near-surface temperature. Consequently, the warming induced by wind turbines is also highly heterogeneous and depends strongly on the local flow configuration.

6.3 Implications for experimental studies

Several in situ experimental studies (San Gorgonio campaign, see Baidya Roy and Traiteur (2010)),(Rajewski et al., 2013, 2016; Henschen et al., 2011; Smith et al., 2013) estimate turbine-induced meteorological variations by computing the difference between measurements from an upstream and a downstream sensor. However, the present results suggest that such approaches may be insufficient in complex flow conditions. In particular, the wake direction at hub height and the advection direction of near-surface meteorological variations can differ significantly in complex terrain.

Furthermore, even in the absence of a wind farm, meteorological properties may evolve substantially between upstream and downstream locations due to natural atmospheric variability. For these reasons, experimental setups should ideally include multiple near-surface meteorological stations distributed around the wind farm (as for the VERTEX campaign of Archer et al. (2019)). Such measurements would help characterize local flows and better distinguish the background atmospheric evolution from the perturbations directly induced by the turbines.

https://doi.org/10.5194/wes-2026-84
Preprint. Discussion started: 20 May 2026
© Author(s) 2026. CC BY 4.0 License.



eawe european academy of wind energy
Open Access WIND ENERGY SCIENCE DISCUSSIONS

7 Conclusions

In an effort to better understand the interactions between wind turbines and a realistic atmosphere, a multiscale modeling framework including atmosphere-soil-vegetation coupling was employed. A case study focusing on the interaction between a stable and strongly stratified atmosphere and the *Ensemble Éolien Catalan* wind farm was analyzed in order to evaluate near-surface meteorological variations induced by wind turbines.

The numerical simulations highlight the major role of topography in shaping the local atmospheric circulation around the wind farm. Under the stable nocturnal conditions, the flow is strongly influenced by terrain-induced circulations, like local katabatic flows that lead to the interaction of air masses with distinct properties. As a result, the near-surface atmosphere already exhibits strong spatial heterogeneity before any interaction with the wind turbines occurs.

After 55 minutes of turbine operation, the averaged meteorological fields from simulations with and without ADR were compared in order to isolate turbine-induced atmospheric perturbations. Inside the wind farm, a mean near-surface warming of approximately 0.4 °C is observed, while localized temperature variations of up to 1.6 °C occur in the immediate vicinity of some turbines. Variation of near ground wind speed is also noted with zones of acceleration and deceleration associated with blockage effects of wind turbine. These near-ground warming anomalies are advected by the local wind which, in the present case, differs by nearly 30–50° from the wind direction at hub height. These atmospheric perturbations impact surface conditions, resulting in ground temperature variations ranging from -0.7 to +1.6 °C, consistent with changes in near-surface air temperature and wind through change in turbulent heat fluxes.

The meteorological variations generated by the wind turbines result from the combination of two main contributions. First, individual turbines produce vertical perturbations associated with wake dynamics. Second, the wind farm behaves as a collective obstacle to the atmospheric circulation that modifies the large-scale flow around the farm altering the local horizontal distribution of air masses. In the present case, the position of a katabatic is locally modified in the vicinity of the wind farm, producing a strong temperature anomalies pattern downstream of the wind farm.

Overall, the results demonstrate that wind farm-atmosphere interactions in complex terrains and under strongly stable conditions are governed by a combination of multiscale processes involving terrain-induced flows, atmospheric stratification, turbine wake and wind farm blockage dynamics. These processes lead to highly heterogeneous meteorological responses near the surface resulting from the superposition of individual turbine wakes and global dynamical influence of the wind farm. This intrinsic complexity also poses a major challenge for both realistic numerical simulations and in situ measurement campaigns, as it complicates the interpretation and generalization of wind farm-atmosphere interactions.

From an applied perspective, the simulated near ground temperature increases within parts of the wind farm are of the same order of magnitude as those produced by frost protection fans used in vineyards. However, the simulations also reveal cooling areas and wind reductions in some regions surrounding the farm, highlighting that the effects of wind turbines on frost conditions may vary significantly depending on the local flow configuration. Moreover, the effectiveness of wind turbines in this context is inherently limited by their operational constraints. If wind speeds at hub height remain below the cut-in wind speed, the turbines do not operate and therefore cannot contribute to atmospheric mixing. This limitation is particularly relevant

https://doi.org/10.5194/wes-2026-84
Preprint. Discussion started: 20 May 2026
© Author(s) 2026. CC BY 4.0 License.



eawe european academy of wind energy
Open Access WIND ENERGY SCIENCE DISCUSSIONS

during radiative cooling events, which are typically associated with weak wind conditions (Snyder and de Melo-Abreu, 2005). In addition, under forecast icing conditions on turbine blades, wind turbines may be shut down to prevent damage caused by ice throw.

Finally, this study illustrates the importance of realistic multiscale numerical simulations for investigating turbine-atmosphere interactions in complex environments. Such approaches provide a unique capability to isolate turbine-induced perturbations from the natural variability of the atmosphere, which remains challenging in observational studies.

The simulations suggest that the orientation of turbine rows relative to the incoming wind direction influences both turbine operation and the advection of near-surface warming. A dedicated sensitivity study could therefore investigate the effect of wind farm layout on near-surface meteorological variations under identical atmospheric conditions, for instance by rotating the wind farm layout.

Finally, to generalize the results presented here, further simulations should be conducted under a wider range of atmospheric conditions. Future work could include cases with different stability regimes, seasons, wind directions, and wind speeds in order to better characterize the range of possible turbine-atmosphere interactions near the surface.

Code availability. The Meso-NH v5.7.1 code is available at (https://zenodo.org/records/15095131), some developments from Meso-NH v6.0.0 (https://zenodo.org/records/19398091) were also used in the present simulations.

Video supplement. A video of the large scale simulation is available at https://doi.org/10.5446/73018. It shows the vertical cross-sections of wind speed at 80 m above ground level from a Meso-NH simulation between 7 and 8 April 2021, centered on the *Ensemble Éolien Catalan* wind farm, located West of Perpignan, France.

Appendix A: Vertical profiles in the Ref small-scale simulation

Figure A1 shows 5-minute averaged vertical profiles at the center of domain D4 in the Ref simulation.

Appendix B: Vertical cross-sections of ADR wakes

Vertical cross-sections along two segments, averaged over 30 minutes, are shown in Fig. B1. Segment AB crosses the wind farm parallel to the mean wind direction and intersects wind turbines 32, 26, and 21. Segment CD is perpendicular to AB and located $1D$ downstream of wind turbine 26, it therefore intersects the wakes of turbines 26, 27, and 24.

https://doi.org/10.5194/wes-2026-84
Preprint. Discussion started: 20 May 2026
© Author(s) 2026. CC BY 4.0 License.

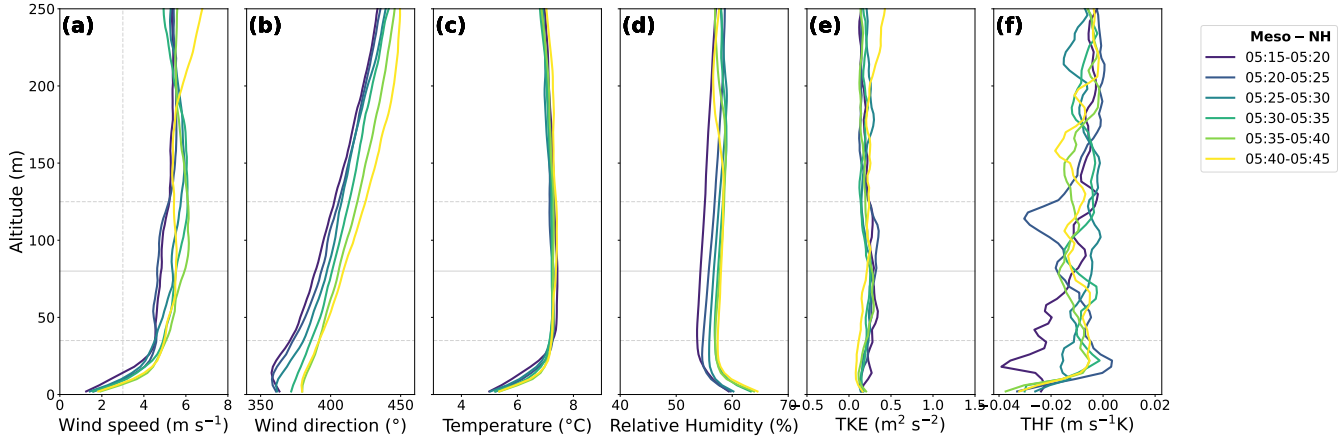


Figure A1. 5-min averaged vertical profiles of (a) Wind speed, (b) Wind direction, (c) Temperature, (d) Relative Humidity (e) TKE, (f) Turbulent heat flux, at the center of the domain D4 for Ref simulation. The wind turbine hub and rotor dimension are represented by solid and dashed grey lines.

https://doi.org/10.5194/wes-2026-84
Preprint. Discussion started: 20 May 2026
© Author(s) 2026. CC BY 4.0 License.

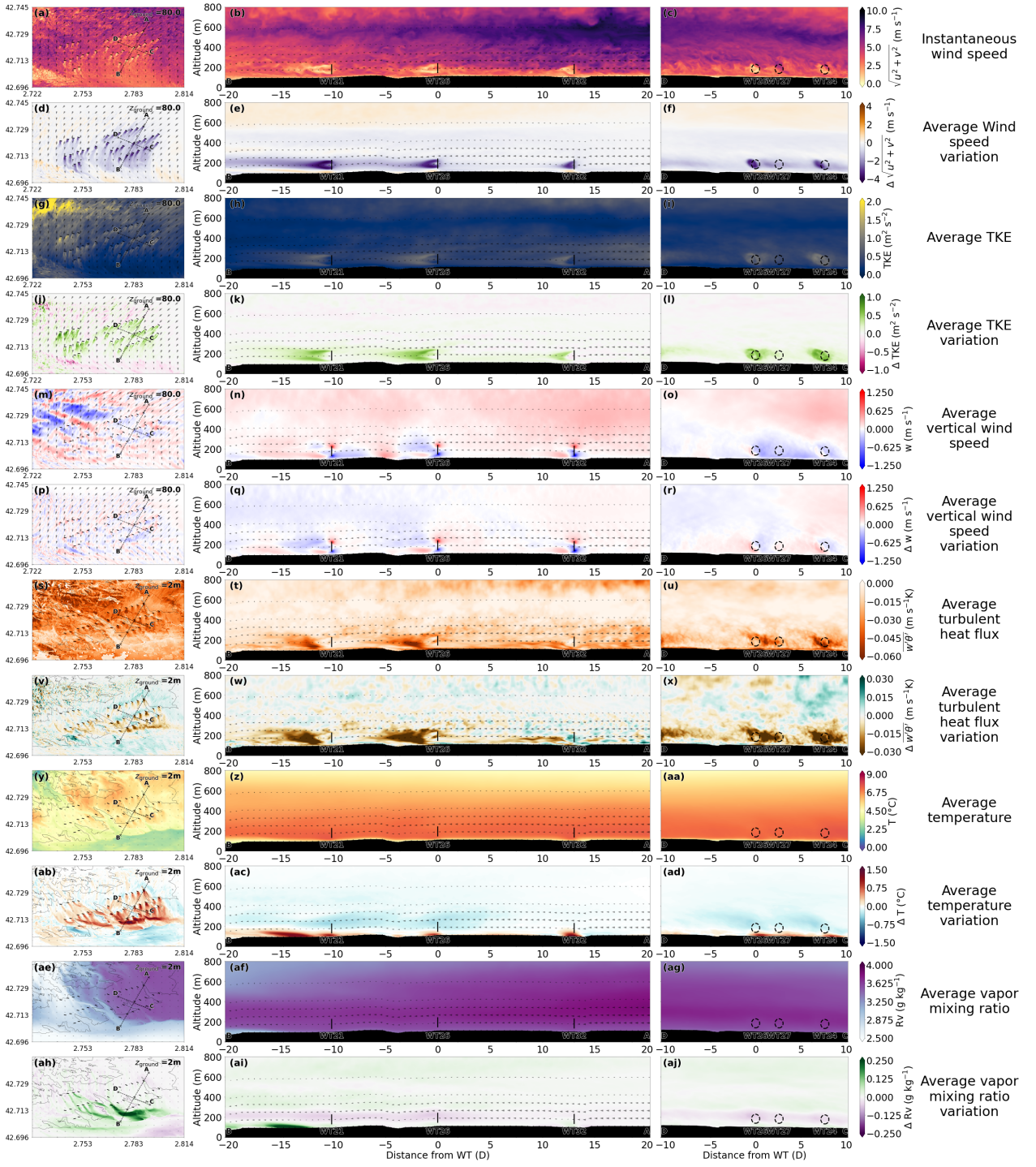


Figure B1. First column : horizontal cross-sections (80 m or at 2 m above the ground), second column : vertical cross-sections along the wake, third column : cross-sections across the wake at 1D downstream of the wind turbine 26. The position of the ADR is represented by a bold black line, and the rotor projection is indicated by a dashed black circle. The terrain is represented in black and altitude zero is equal to sea level.

https://doi.org/10.5194/wes-2026-84
Preprint. Discussion started: 20 May 2026
© Author(s) 2026. CC BY 4.0 License.



eawe european academy of wind energy
Open Access WIND ENERGY SCIENCE DISCUSSIONS

The structure, shape, and length of the wakes deficits (Fig. B1 d,e,f) differ from those typically observed in idealized large-eddy simulations. These differences arise because the simulations are conducted under realistic atmospheric conditions, in which the horizontal wind direction varies within the farm, preventing the cross-sections from passing exactly through the wake centers of all three turbines. In addition, the results are averaged over 30 minutes, during which both wind direction and turbine yaw angle vary slightly, contributing to a spreading of the wakes in the averaged fields. The wind direction is also strongly vertically stratified (see Fig. A1b), leading to vertically sheared flow conditions. This vertical shear induces a pronounced stretching and distortion of the wakes with height. Finally, the complex topography within the wind farm generates additional turbulent, vertical movement and chaotic air motions that further disrupt wake coherence and enhance wake deformation and recovery (Mi et al., 2025).

Instantaneous wind fields reveal velocity fluctuations and vertical structures. This turbulence is explained by the synoptic and mesoscale circulation context, including the interaction between different air masses, strong vertical wind shear, and complex terrain that induces vertical motions. Wind turbines interact with this ambient turbulence, while wake velocity deficits and wake rotation further enhance turbulent motions within the flow. As it is commonly reported in LES studies (Xie and Archer, 2017; Boumendil et al., 2025), the additional TKE generated in the wake is larger in the upper than in the lower part of the wake (Fig. B1k).

The vertical wind component w, indicates strong vertical motions both near the surface and aloft (Fig. B1n). These vertical exchanges result from the convergence of air masses combined with the influence of complex terrain. The wind farm adds further vertical motions (Fig. B1q) to this already disturbed atmosphere. Individual turbine-induced motions can be distinguished on the 3D iso surface plot (Fig. C2), the typical Ying-Yang shape with upward vertical motion on the upper and right part of the rotor and the downward motion on the lower and left part of the rotor generated by wake rotation and induction effects (Lu and Porté-Agel, 2011; Mirocha et al., 2014; Boumendil et al., 2024).

Upward and downward vertical motions in the rotor region transport relatively cooler air masses above the rotor and warmer air masses near the surface (Fig. C3). The amplitude of the resulting temperature anomalies is larger near the ground because the strong stable temperature inversion causes even small vertical displacements to mix air masses with markedly different temperatures. Furthermore, due to the strong vertical wind shear associated with the stratified atmosphere, the advection direction of the temperature anomalies differ significantly above and below the rotor.

Under stable atmospheric conditions, the turbulent heat flux is negative. At night, radiative cooling of the surface makes the ground colder than the air above, creating a temperature inversion. As a result, heat is transported downward by turbulence, from the relatively warmer air toward the colder surface, leading to a negative turbulent heat flux. Within the wind turbine wake, an increase in the magnitude of the turbulent heat flux is observed, making it even more negative. This indicates an enhanced downward transport of heat caused by wake-generated turbulence, which intensifies mixing despite the stable stratification.

https://doi.org/10.5194/wes-2026-84
Preprint. Discussion started: 20 May 2026
© Author(s) 2026. CC BY 4.0 License.



eawe european academy of wind energy
Open Access WIND ENERGY SCIENCE DISCUSSIONS

B1 3D iso-surfaces

Figures C1, C2, C3 respectively show the 3D iso-surfaces of wind speed deficit, vertical wind velocity, and temperature variation within the subdomain, all viewed from the same perspective. These visualizations provide a spatial representation of the different perturbations induced by the wind turbines.

The vertical motions generated by the turbines are primarily confined to the immediate vicinity of the ADR. These effects are also visible upstream of the turbines, within the induction zone. In contrast, the wind speed deficit wakes extend much further downstream. Additionally, upstream turbine rows generate a wind deficit that impacts downstream turbines.

The temperature variation field highlights a clear vertical structure. Near the surface, localized warming zones are observed, whereas cooling regions develop above the rotor area. Due to the strong wind veer, the advection of these temperature anomalies differs significantly from the wake direction. Near-surface warming is advected toward the left, while cooling aloft is advected toward the right. Furthermore, the magnitude of the warming is significantly larger than that of the cooling.

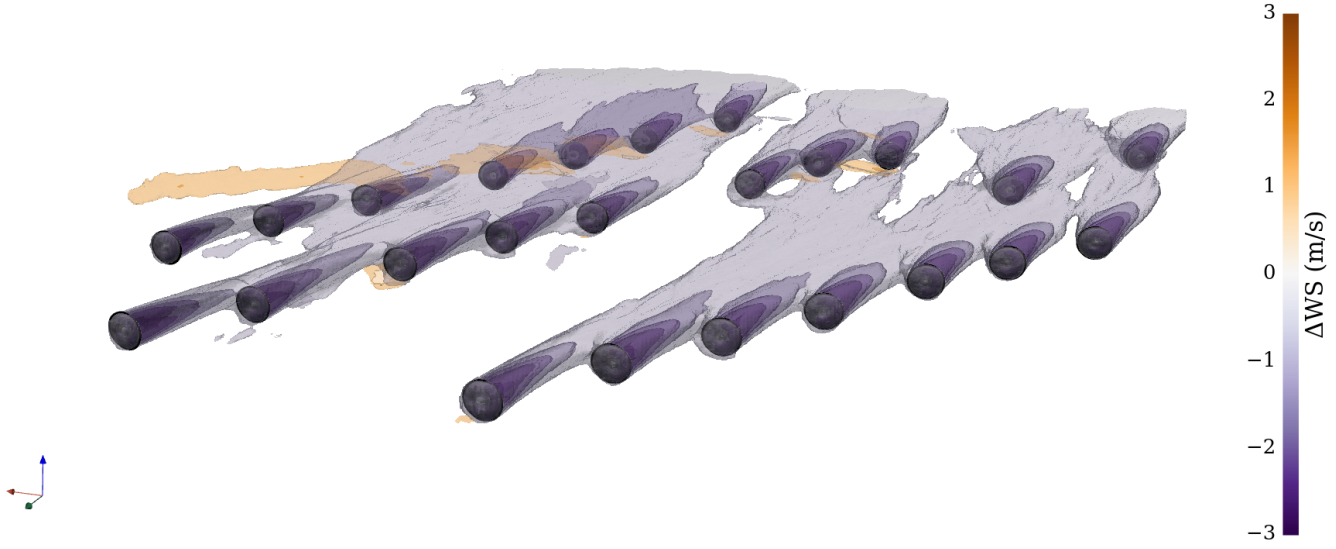


Figure C1. 3D iso-surface of the wind speed deficit in the subdomain

https://doi.org/10.5194/wes-2026-84
Preprint. Discussion started: 20 May 2026
© Author(s) 2026. CC BY 4.0 License.

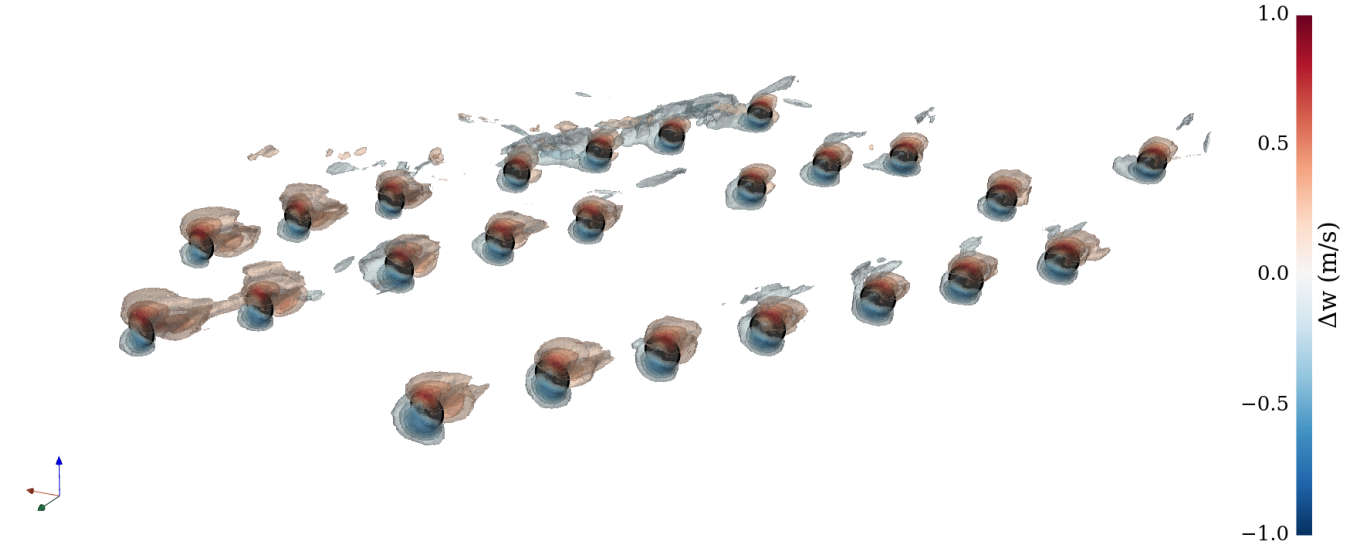


Figure C2. 3D iso-surface of the vertical wind speed in the subdomain

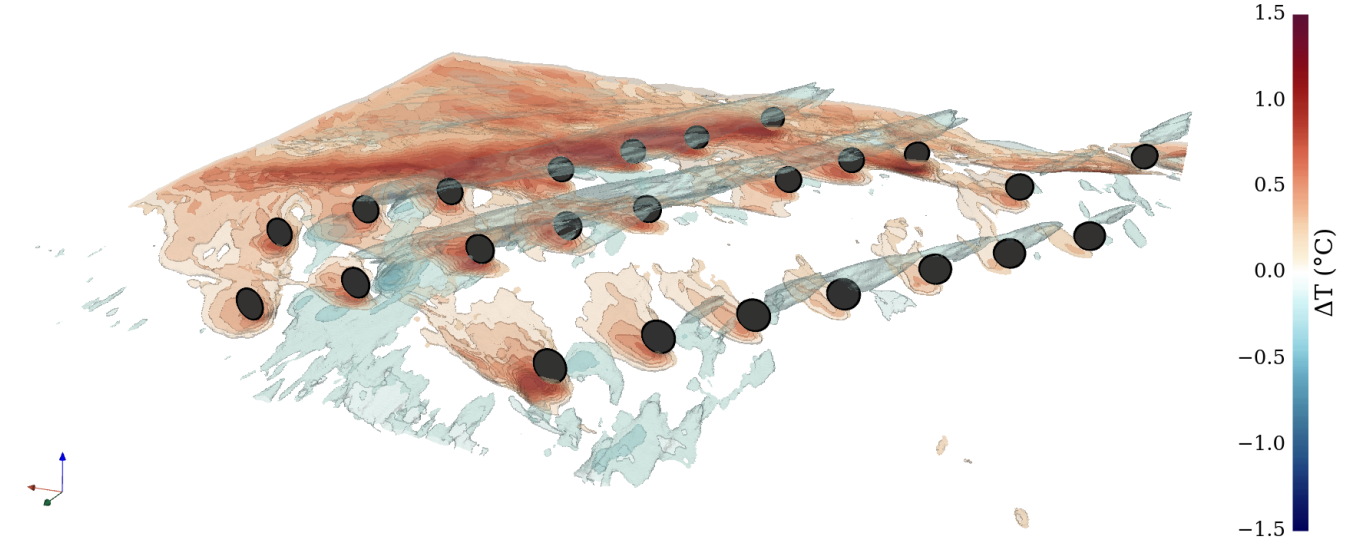


Figure C3. 3D iso-surface of the temperature variation in the subdomain

https://doi.org/10.5194/wes-2026-84
Preprint. Discussion started: 20 May 2026
© Author(s) 2026. CC BY 4.0 License.



eawe european academy of wind energy
Open Access WIND ENERGY SCIENCE DISCUSSIONS

Author contributions. PB performed the simulations, developed the code, and carried out the post-processing and analysis under the supervision of PAJ, QR and VM. PB prepared the initial draft of the article. All authors reviewed and edited the article.

Competing interests. The authors declare that they have no competing interests.

Acknowledgements. Map data are copyrighted by OpenStreetMap contributors and are available at https://www.openstreetmap.org. Computational resources were provided by the Belenos supercomputing facility operated by Météo-France. The authors acknowledge the use of meteorological data from the RADOME station network and the AROME model developed by Météo-France. The authors thank Jean Wurtz, Robert Schotter, Tim Nagel, Marie Minvielle, Fleur Couvreux and Tanguy Lunel for helpful discussions, technical support and for providing some codes and scripts used in this work. The authors acknowledge the use of generative artificial intelligence tools to assist with language editing and support the writing process, as well as to contribute to the development and debugging of scripts used in the post-processing of some figures. All scientific content, analysis, and conclusions remain the responsibility of the authors.

https://doi.org/10.5194/wes-2026-84
Preprint. Discussion started: 20 May 2026
© Author(s) 2026. CC BY 4.0 License.



eawe european academy of wind energy
Open Access WIND ENERGY SCIENCE DISCUSSIONS

References

Adkins, K. A. and Sescu, A.: Observations of relative humidity in the near-wake of a wind turbine using an instrumented unmanned aerial system, International Journal of Green Energy, 14, 845–860, https://doi.org/https://doi.org/10.1080/15435075.2017.1334661, 2017.

Adkins, K. A. and Sescu, A.: Analysis of near–surface relative humidity in a wind turbine array boundary layer using an instrumented unmanned aerial system and large–eddy simulation, Wind Energy, 21, 1155–1168, https://doi.org/10.1002/we.2220, 2018.

Archer, C. L., Wu, S., Vasel-Be-Hagh, A., Brodie, J. F., Delgado, R., St. Pé, A., Oncley, S., and Semmer, S.: The VERTEX field campaign: observations of near-ground effects of wind turbine wakes, Journal of Turbulence, 20, 64–92, https://doi.org/10.1080/14685248.2019.1572161, 2019.

Armstrong, A., Waldron, S., Whitaker, J., and Ostle, N. J.: Wind farm and solar park effects on plant-soil carbon cycling: uncertain impacts of changes in ground-level microclimate, Global change biology, 20, 1699–1706, https://doi.org/https://doi.org/10.1111/gcb.12437, 2014.

Baidya Roy, S.: Simulating impacts of wind farms on local hydrometeorology, Journal of Wind Engineering and Industrial Aerodynamics, 99, 491–498, https://doi.org/https://doi.org/10.1016/j.jweia.2010.12.013, 2011.

Baidya Roy, S. and Traiteur, J. J.: Impacts of wind farms on surface air temperatures, Proceedings of the National Academy of Sciences of the United States of America, 107, 17 899–17 904, https://doi.org/10.1073/pnas.1000493107, 2010.

Baidya Roy, S., Pacala, S. W., and Walko, R. L.: Can large wind farms affect local meteorology?, Journal of Geophysical Research: Atmospheres, 109, https://doi.org/10.1029/2004JD004763, 2004.

Bakhoday-Paskyabi, M., Krutova, M., Bui, H., and Ning, X.: Multiscale Simulation of Offshore Wind Variability During Frontal Passage: Brief Implication on Turbines' Wakes and Load, Journal of Physics: Conference Series, 2362, 012 003, https://doi.org/10.1088/1742-6596/2362/1/012003, 2022.

Bocher, E., Bernard, J., Wiederhold, E., Leconte, F., Petit, G., Palominos, S., and Noûs, C.: GeoClimate: a Geospatial processing toolbox for environmental and climate studies, Journal of Open Source Software, 6, 3541, https://doi.org/https://doi.org/10.21105/joss.03541, 2021.

Boone, A., Masson, V., Meyers, T., and Noilhan, J.: The Influence of the Inclusion of Soil Freezing on Simulations by a Soil–Vegetation–Atmosphere Transfer Scheme, Journal of Applied Meteorology, 39, 1544–1569, https://doi.org/10.1175/1520-0450(2000)039<1544:TIOTIO>2.0.CO;2, 2000.

Boumendil, P., Joulin, P.-A., Toumi, H. Z., Rodier, Q., and Masson, V.: Role of rotational and divergence effects induced by wind turbines wakes on near-ground air warming, Journal of Physics: Conference Series, 2767, 092 006, https://doi.org/10.1088/1742-6596/2767/9/092006, 2024.

Boumendil, P., Rodier, Q., Joulin, P.-A., and Masson, V.: A multi-scale model with an atmosphere - soil - vegetation coupling to explore the effect of wind turbines on near-surface meteorological conditions, Journal of Physics: Conference Series, 3016, 012 002, https://doi.org/10.1088/1742-6596/3016/1/012002, 2025.

Caniaux, G., Redelsperger, J.-L., and Lafore, J.-P.: A Numerical Study of the Stratiform Region of a Fast-Moving Squall Line. Part I: General Description and Water and Heat Budgets, Journal of the Atmospheric Sciences, 51, 2046–2074, https://doi.org/https://doi.org/10.1175/1520-0469(1994)051<2046:ANSOTS>2.0.CO;2, 1994.

Cuxart, J., Bougeault, P., and Redelsperger, J.-L.: A turbulence scheme allowing for mesoscale and large–eddy simulations, Quarterly Journal of the Royal Meteorological Society, 126, 1–30, https://doi.org/10.1002/qj.49712656202, 2000.

https://doi.org/10.5194/wes-2026-84
Preprint. Discussion started: 20 May 2026
© Author(s) 2026. CC BY 4.0 License.

Decharme, B., Boone, A., Delire, C., and Noilhan, J.: Local evaluation of the Interaction between Soil Biosphere Atmosphere soil multilayer diffusion scheme using four pedotransfer functions, Journal of Geophysical Research: Atmospheres, 116, https://doi.org/10.1029/2011JD016002, 2011.

Durran, D. R.: Improving the Anelastic Approximation, Journal of the Atmospheric Sciences, 46, 1453–1461, 1989.

Faroux, S., Kaptué Tchuenté, A. T., Roujean, J.-L., Masson, V., Martin, E., and Le Moigne, P.: ECOCLIMAP-II/Europe: a twofold database of ecosystems and surface parameters at 1 km resolution based on satellite information for use in land surface, meteorological and climate models, Geoscientific Model Development, 6, 563–582, https://doi.org/10.5194/gmd-6-563-2013, 2013.

Henschen, M., Herrholtz, B., Rhudy, L., Demchak, K., Doogs, B., Holland, J., Larson, E., Martin, J., and Rudkin, M.: Do Wind Turbines Affect Weather Conditions: A Case Study in Indiana, Journal of Purdue Undergraduate Research, 1, 22–29, https://doi.org/https://doi.org/10.5703/jpur.01.1.4, 2011.

Hogan, R. J. and Bozzo, A.: A Flexible and Efficient Radiation Scheme for the ECMWF Model, Journal of Advances in Modeling Earth Systems, 10, 1990–2008, https://doi.org/https://doi.org/10.1029/2018MS001364, 2018.

Honnert, R., Masson, V., Lac, C., and Nagel, T.: A Theoretical Analysis of Mixing Length for Atmospheric Models From Micro to Large Scales, Frontiers in Earth Science, 8, https://doi.org/https://doi.org/10.3389/feart.2020.582056, 2021.

Joulin, P.-A., Mayol, M. L., Masson, V., Blondel, F., Rodier, Q., Cathelain, M., and Lac, C.: The Actuator Line Method in the Meteorological LES Model Meso-NH to Analyze the Horns Rev 1 Wind Farm Photo Case, Frontiers in Earth Science, 7, https://doi.org/https://doi.org/10.3389/feart.2019.00350, 2020.

Kaffine, D. T.: Microclimate effects of wind farms on local crop yields, Journal of Environmental Economics and Management, 96, 159–173, https://doi.org/https://doi.org/10.1016/j.jeem.2019.06.001, 2019.

Kale, B., Buckingham, S., van Beeck, J., and Cuerva-Tejero, A.: Multi-scale modeling of a wind turbine wake in complex terrain, Journal of Physics: Conference Series, 2505, 012 012, https://doi.org/10.1088/1742-6596/2505/1/012012, 2023.

Keith, D. W., Decarolis, J. F., Denkenberger, D. C., Lenschow, D. H., Malyshev, S. L., Pacala, S., and Rasch, P. J.: The influence of large-scale wind power on global climate, Proceedings of the National Academy of Sciences of the United States of America, 101, 16 115–16 120, https://doi.org/https://doi.org/10.1073/pnas.0406930101, 2004.

Lac, C., Chaboureau, J.-P., Masson, V., Pinty, J.-P., Tulet, P., Escobar, J., Leriche, M., Barthe, C., Aouizerats, B., Augros, C., Aumond, P., Auguste, F., Bechtold, P., Berthet, S., Bielli, S., Bosseur, F., Caumont, O., Cohard, J.-M., Colin, J., Couvreux, F., Cuxart, J., Delautier, G., Dauhut, T., Ducrocq, V., Filippi, J.-B., Gazen, D., Geoffroy, O., Gheusi, F., Honnert, R., Lafore, J.-P., Lebeaupin Brossier, C., Libois, Q., Lunet, T., Mari, C., Maric, T., Mascart, P., Mogé, M., Molinié, G., Nuissier, O., Pantillon, F., Peyrillé, P., Pergaud, J., Perraud, E., Pianezze, J., Redelsperger, J.-L., Ricard, D., Richard, E., Riette, S., Rodier, Q., Schoetter, R., Seyfried, L., Stein, J., Suhre, K., Taufour, M., Thouron, O., Turner, S., Verrelle, A., Vié, B., Visentin, F., Vionnet, V., and Wautelet, P.: Overview of the Meso-NH model version 5.4 and its applications, Geoscientific Model Development, 11, 1929–1969, https://doi.org/10.5194/gmd-11-1929-2018, 2018.

Lamichhane, J. R.: Rising risks of late-spring frosts in a changing climate, Nature Climate Change, 11, 554–555, https://doi.org/10.1038/s41558-021-01090-x, 2021.

Le Cap, C., Carlier, J., Quénol, H., Heitz, D., and Buisson, E.: Analysis of the spatial variability of temperature with the aim of improving the location of wind machines, Theoretical and Applied Climatology, 155, 421–438, https://doi.org/10.1007/s00704-023-04642-7, 2024.

Lemoine, A. and Pineaud, A.: Bulletin climatique avril 2021, https://donneespubliques.meteofrance.fr/donnees_libres/bulletins/BCM/202104.pdf, 2021.

https://doi.org/10.5194/wes-2026-84
Preprint. Discussion started: 20 May 2026
© Author(s) 2026. CC BY 4.0 License.



Lu, H. and Porté-Agel, F.: Large-eddy simulation of a very large wind farm in a stable atmospheric boundary layer, Physics of Fluids, 23, https://doi.org/https://doi.org/10.1063/1.3589857, 2011.

Masson, V.: A Physically-Based Scheme For The Urban Energy Budget In Atmospheric Models, Boundary-Layer Meteorology, 94, 357–397, https://doi.org/10.1023/A:1002463829265, 2000.

Masson, V., Le Moigne, P., Martin, E., Faroux, S., Alias, A., Alkama, R., Belamari, S., Barbu, A., Boone, A., Bouyssel, F., Brousseau, P., Brun, E., Calvet, J.-C., Carrer, D., Decharme, B., Delire, C., Donier, S., Essaouini, K., Gibelin, A.-L., Giordani, H., Habets, F., Jidane, M., Kerdraon, G., Kourzeneva, E., Lafaysse, M., Lafont, S., Lebeaupin Brossier, C., Lemonsu, A., Mahfouf, J.-F., Marguinaud, P., Mokhtari, M., Morin, S., Pigeon, G., Salgado, R., Seity, Y., Taillefer, F., Tanguy, G., Tulet, P., Vincendon, B., Vionnet, V., and Voldoire, A.: The SURFEXv7.2 land and ocean surface platform for coupled or offline simulation of earth surface variables and fluxes, Geoscientific Model Development, 6, 929–960, https://doi.org/https://doi.org/10.5194/gmd-6-929-2013, 2013.

Mi, L., Li, B., Chen, H., Zhang, C., Han, Y., and Cai, C. S.: Multiscale coupling wake simulations for a horizontal-axis wind turbine mounted in complex terrains, Energy Sources, Part A: Recovery, Utilization, and Environmental Effects, 47, 1817–1835, https://doi.org/https://doi.org/10.1080/15567036.2025.2449980, 2025.

Mirocha, J. D., Kosovic, B., Aitken, M. L., and Lundquist, J. K.: Implementation of a generalized actuator disk wind turbine model into the weather research and forecasting model for large-eddy simulation applications, Journal of Renewable and Sustainable Energy, 6, https://doi.org/https://doi.org/10.1063/1.4861061, 2014.

OpenStreetMap contributors: Planet dump retrieved from https://planet.osm.org , https://www.openstreetmap.org, 2017.

Pergaud, J., Masson, V., Malardel, S., and Couvreux, F.: A Parameterization of Dry Thermals and Shallow Cumuli for Mesoscale Numerical Weather Prediction, Boundary-Layer Meteorology, 132, 83–106, https://doi.org/10.1007/s10546-009-9388-0, 2009.

Pinty, J.-P. and Jabouille, P.: A mixed-phase cloud parameterization for use in a mesoscale non-hydrostatic model: Simulations of a squall line of orographic precipitation, 1998.

Porté-Agel, F., Bastankhah, M., and Shamsoddin, S.: Wind-Turbine and Wind-Farm Flows: A Review, Boundary-Layer Meteorology, 174, 1–59, https://doi.org/https://doi.org/10.1007/s10546-019-00473-0, 2020.

Qin, Y., Li, Y., Xu, R., Hou, C., Armstrong, A., Bach, E., Wang, Y., and Fu, B.: Impacts of 319 wind farms on surface temperature and vegetation in the United States, Environmental Research Letters, 17, 024 026, https://doi.org/10.1088/1748-9326/ac49ba, 2022.

Quint, D., Lundquist, J. K., Bodini, N., and Rosencrans, D.: Simulated meteorological impacts of offshore wind turbines and sensitivity to the amount of added turbulence kinetic energy, Wind Energy Science, 10, 1269–1301, https://doi.org/10.5194/wes-10-1269-2025, 2025.

Rajewski, D. A., Takle, E. S., Lundquist, J. K., Oncley, S., Prueger, J. H., Horst, T. W., Rhodes, M. E., Pfeiffer, R., Hatfield, J. L., Spoth, K. K., and Doorenbos, R. K.: Crop Wind Energy Experiment (CWEX): Observations of Surface-Layer, Boundary Layer, and Mesoscale Interactions with a Wind Farm, Bulletin of the American Meteorological Society, 94, 655–672, https://doi.org/https://doi.org/10.1175/BAMS-D-11-00240.1, 2013.

Rajewski, D. A., Takle, E. S., Prueger, J. H., and Doorenbos, R. K.: Toward understanding the physical link between turbines and microclimate impacts from in situ measurements in a large wind farm, Journal of Geophysical Research: Atmospheres, 121, https://doi.org/https://doi.org/10.1002/2016JD025297, 2016.

Rasheed, A., Tabib, M., and Kristiansen, J.: Wind Farm Modeling in a Realistic Environment Using a Multiscale Approach, in: Volume 10: Ocean Renewable Energy, American Society of Mechanical Engineers, ISBN 978-0-7918-5778-6, https://doi.org/10.1115/omae2017-61686, 2017.

https://doi.org/10.5194/wes-2026-84
Preprint. Discussion started: 20 May 2026
© Author(s) 2026. CC BY 4.0 License.

Smith, C. M., Barthelmie, R. J., and Pryor, S. C.: In situ observations of the influence of a large onshore wind farm on near-surface temperature, turbulence intensity and wind speed profiles, Environmental Research Letters, 8, 034 006, https://doi.org/10.1088/1748-9326/8/3/034006, 2013.

Snyder, R. L. and de Melo-Abreu, J. P.: Frost protection: Fundamentals, practice and economics, vol. no. 10 of *Environment and natural resources series*, Food and Agriculture Organization of the United Nations, Rome, ISBN 92-5-105328-6, 2005.

Tang, B., Wu, D., Zhao, X., Zhou, T., Zhao, W., and Wei, H.: The Observed Impacts of Wind Farms on Local Vegetation Growth in Northern China, Remote Sensing, 9, 332, https://doi.org/https://doi.org/10.3390/rs9040332, 2017.

Tardieu, J. and Leroy, M.: Radome, le réseau temps réel d'observation au sol de Météo-France, La Météorologie, 8, 40, https://doi.org/10.4267/2042/36262, 2003.

Urziceanu, M., Anastasiu, P., Rozylowicz, L., and Sesan, T. E.: Local-scale impact of wind energy farms on rare, endemic, and threatened plant species, PeerJ, 9, e11 390, https://doi.org/10.7717/peerj.11390, 2021.

Wang, Q., Luo, K., Yuan, R., Wang, S., Fan, J., and Cen, K.: A multiscale numerical framework coupled with control strategies for simulating a wind farm in complex terrain, Energy, 203, 117 913, https://doi.org/10.1016/j.energy.2020.117913, 2020.

Wise, A. S., Neher, J. M. T., Arthur, R. S., Mirocha, J. D., Lundquist, J. K., and Chow, F. K.: Meso- to microscale modeling of atmospheric stability effects on wind turbine wake behavior in complex terrain, Wind Energy Science, 7, 367–386, https://doi.org/https://doi.org/10.5194/wes-7-367-2022, 2022.

Wu, S. and Archer, C. L.: Near-Ground Effects of Wind Turbines: Observations and Physical Mechanisms, Monthly Weather Review, 149, 879–898, https://doi.org/10.1175/MWR-D-20-0186.1, 2021.

Wu, S., Archer, C. L., and Mirocha, J. D.: New insights on wind turbine wakes from large–eddy simulation: Wake contraction, dual nature, and temperature effects, Wind Energy, https://doi.org/https://doi.org/10.1002/we.2827, 2023.

Wu, Y.-T. and Porté-Agel, F.: Large-Eddy Simulation of Wind-Turbine Wakes: Evaluation of Turbine Parametrisations, Boundary-Layer Meteorology, 138, 345–366, https://doi.org/10.1007/s10546-010-9569-x, 2011.

Xie, S. and Archer, C. L.: A Numerical Study of Wind-Turbine Wakes for Three Atmospheric Stability Conditions, Boundary-Layer Meteorology, 165, 87–112, https://doi.org/10.1007/s10546-017-0259-9, 2017.

Zhou, L., Tian, Y., Baidya Roy, S., Thorncroft, C., Bosart, L. F., and Hu, Y.: Impacts of wind farms on land surface temperature, Nature Climate Change, 2, 539–543, https://doi.org/10.1038/nclimate1505, 2012.